PC4199 : Honours Project in Physics

A Fast Polarization Independent Phase Shifter Of Light

Student : Ng Tien Tjuen

Supervisor : A/P Christian Kurtsiefer & Asst/P Antia Lamas Linares

A thesis submitted to the Department of Physics

in partial fulfillment of the requirements for the degree of

Bachelor of Science (Honours)

Semester I & II 2006/2007

Acknowledgements

I would like to thank my project supervisors A/P Christian Kurtsiefer and Asst/P Antia Lamas Linares for their fully supports, inspiring ideas and encouragement. I appreciate their valuable advice, discussions and guidance given to me while doing my undergraduate thesis.

Thanks to my partner, Darwin Gosal for his help in this project when I was completely busy in my coursework studies. Thanks to Hou Shun, Meng Khoon, Zilong, Alexander Ling and etc in the group for their practical advice and helps. Without their assistance, I would not make any further progress during this period.

Finally, I'd like to thank my family and friends for getting me this far and providing the necessary supports and advice on all life's problems.

Ng Tien Tjuen

Singapore, March 2007

Abstract

A high speed Y cut Lithium Niobate ($LiNbO_3$) electro optic modulator for visible wavelength operation has been characterized. The bulk phase modulator exhibits incoming light polarization free dependency. By utilizing the interference effect of a Mach Zehnder interferometer, the π phase shift corresponds to a half wave voltage across the crystal could be accurately measured. The measured half wave voltage and a visibility for a 633nm laser wavelength were (96±2)V and 96%. The experimental setup consisting of a phase modulator and interferometer would be a high speed light shutter. The light shutter is able to switch the laser beam on or off in less than 2ns with a repetition rate of 100kHz. In the electronic switching circuit, the shutter switching time is achieved by using a MOSFET. The MOSFET discharges the voltage across the crystal in less than 2ns, thereby the light undergoes phase shift and this gives rise to the interference effect. The interferometer would be an ideal design for a fast optical shutter and it has the advantages of incoming light polarization independent and easy to construct.

Contents

Chapter 1

Introduction

Light modulation is one of the effects when the light passes through the anisotropic crystal. A controllable optical property of an anisotropic crystal gives us a better control of the light modulation. Setting up a fast phase modulation of light experiment based on electro optic effect is the task of this project. This is the effect whereby the optical properties are changed when the anisotropic crystal is subjected to an external electric field. Devices based on these phenomena have been used for the control of light for more than a century. But it was the discovery of the laser in 1960s that stimulated most of the recent studies and applications of these effects[1].

The special feature of the electro optic phase modulator built in this project is the phase modulation is independent of the polarization of light sent into the modulator. Most of the commercial products available are polarization dependent devices because of the anisotropic crystals inside the modulator. A new scheme has been implemented to come out with a phase modulator using the same anisotropic crystal but the device is polarization independent.

The motivation of this project is to rely upon of the phase shift of the light to set up a laser light shutter. The laser light could be turned on or off by utilizing the interference effect

of a Mach Zehnder interferometer. The phase difference between the two laser beams gives rise to the interference. Mechanical shutters[2] and moving mirrors have too much inertia to permit the modulation at the frequencies range from megahertz to gigahertz. Therefore, it is necessary to rely upon optical interaction with electrical field at the modulating frequency via the nonlinearities of matter. In fact, the light shutter consisting of a electro optic modulator and a high speed electronic switch were reported[3], but that device is not polarization independent. Furthermore that element has significant attenuation for the light. Hence, this project tries to implement polarization independent switching with a fast modulation and low losses.

We begin with the concepts of propagation of optical waves inside the crystal and the electro optic effect in chapter 2. Following that, in chapter 3, we discuss the experimental setup and the phase shift measurement. In chapter 4, we present some general practical considerations in the electro optic modulator. The fast switching circuit design will be discussed in chapter 5. Results and analysis of the modulation are presented in chapter 6. Finally, the last chapter would be the conclusions and some future work to be done.

Chapter 2

Optical Waves In Crystals

2.1 Optics of Anisotropic Media

An anisotropic medium has its macroscopic optical properties depend on the polarization of light. If the molecules are orientated in the same direction and organized in space according to regular periodic positions, the medium is in general anisotropic. The electromagnetic of anisotropic media and the propagation of optical radiation in crystals in the presence of an applied electric field will be discussed here. The index of refraction can be changed when subjected to an external electric field, this is referred to as the electro optic effect. The change in the refractive index is typically very small but it gives a very significant phase modulation. If the changes in the refractive indices are proportional to the applied electric field, such an effert is known as the Pockel effect or linear electro optic effect. This effect will be discussed in the later part of this chapter. The expressions for the change of refractive index upon acted by an external electric field will be derived. Consequently, the expressions lead to a clear picture how does the modulation effect is polarization dependent.

2.1.1 Propagation of Electromagnetic Waves In Anisotropic Crystals

In an anisotropic crystal, the polarization induced by an external electric field and the field itself are not always parallel. Each component of the electric flux density $\mathbf{D}$ in a linear anisotropic dielectric medium is a linear combination of the three components of the electric field

$$D_k = \varepsilon_{kl} E_l \tag{2.1}$$

where $k, l = 1, 2, 3$ indicate the x, y, and z components respectively. The dielectric properties of the medium are characterized by a 3×3 array of nine coefficients ε_{kl} forming a tensor of second rank known as the electric permittivity tensor and denoted by ϵ. Equation (2.1) is written in the symbolic form $\mathbf{D} = \epsilon \mathbf{E}$.

Considering the stored electric energy density as in an isotropic medium[4],

$$\omega_e = \frac{1}{2}\mathbf{D} \cdot \mathbf{E} = \frac{1}{2} E_k \varepsilon_{kl} E_l \tag{2.2}$$

The time derivative of $\dot{\omega}_e$ is

$$\dot{\omega}_e = \frac{\varepsilon_{kl}}{2}(\dot{E}_k E_l + E_k \dot{E}_l) \tag{2.3}$$

Poynting theorem shows the net power flow into a unit volume is

$$-\nabla \cdot (\mathbf{E} \times \mathbf{H}) = \mathbf{E} \cdot \dot{\mathbf{D}} + \mathbf{H} \cdot \dot{\mathbf{B}} \tag{2.4}$$

From (2.1), (2.4) can be written as

$$-\nabla \cdot (\mathbf{E} \times \mathbf{H}) = E_k \varepsilon_{kl} \dot{E}_l + \mathbf{H} \cdot \dot{\mathbf{B}} \tag{2.5}$$

If the Poynting vector is to correspond to the energy flux in anisotropic media, as it does in the isotropic ones, then the first term on the right side of (2.5) must be equal to $\dot{\omega}_e$ and it is same as $\dot{\omega}_e$ given by (2.3). Expressing $E_k \varepsilon_{kl} \dot{E}_l$ as

$$\dot{\omega}_e = \frac{1}{2}(\varepsilon_{lk}\dot{E}_k E_l + \varepsilon_{kl} E_k \dot{E}_l) \tag{2.6}$$

and compare to (2.3), it follows that

$$\varepsilon_{lk} = \varepsilon_{lk} \tag{2.7}$$

The electric permittivity tensor is symmetrical and is characterized by only six independent numbers. For certain symmetrical crystals, some of these six coefficients vanish and some are related. From (2.1) and (2.2)

$$2\omega_e = \varepsilon_{xx}E_x^2 + \varepsilon_{yy}E_y^2 + \varepsilon_{zz}E_z^2 + 2\varepsilon_{yz}EyEz + 2\varepsilon_{xz}E_xE_z + 2\varepsilon_{xy}E_xE_y \tag{2.8}$$

A principal axis transformation diagonalize (2.8). In the new coordinate system, ω_e becomes

$$2\omega_e = \varepsilon_x E_x^2 + \varepsilon_y E_y^2 + \varepsilon_z E_z^2 \tag{2.9}$$

with the x, y, z symbols refer to the new axes called *principal dielectric axes.* The tensor ε_{kl} is diagonal and is given by

$$\begin{pmatrix} D_x \\ D_y \\ D_z \end{pmatrix} = \begin{pmatrix} \varepsilon_x & 0 & 0 \\ 0 & \varepsilon_y & 0 \\ 0 & 0 & \varepsilon_z \end{pmatrix} \begin{pmatrix} E_x \\ E_y \\ E_z \end{pmatrix}$$

It follows that

$$2\omega_e = \frac{D_x^2}{\varepsilon_x} + \frac{D_y^2}{\varepsilon_y} + \frac{D_z^2}{\varepsilon_z} \tag{2.10}$$

The constant energy surfaces in the space D_x, D_y, D_z are ellipsoids.

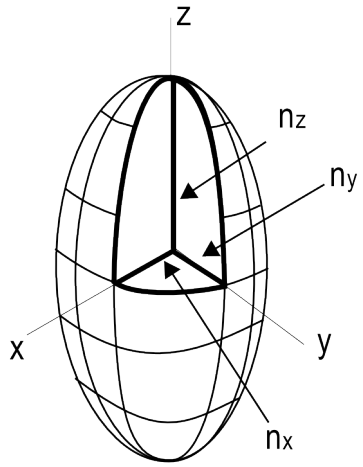

Figure 2.1: The index ellipsoid associated with the refractive indices.

2.1.2 Index Ellipsoid

The constant energy surfaces in **D** space can be written as

$$2\omega_e\varepsilon_0 \;=\; \frac{D_x^2}{\varepsilon'_x}+\frac{D_y^2}{\varepsilon'_y}+\frac{D_z^2}{\varepsilon'_z} \tag{2.11}$$

where $\varepsilon'_x, \varepsilon'_y, \varepsilon'_z$ are the relative principal dielectric constants. By replacing $\frac{\mathbf{D}}{\sqrt{2\omega_e\varepsilon_0}}$ by $\mathbf{r}$ and define the principal indices of refraction n_x, n_y, n_z where $n_k^2 \equiv \varepsilon'_k$, (2.11) can be transformed to

$$\frac{x^2}{n_x^2}+\frac{y^2}{n_y^2}+\frac{z^2}{n_z^2} \;=\; 1 \tag{2.12}$$

This is the equation of a general ellipsoid with major axes parallel to the x, y, z directions whose respective lengths are $2n_x, 2n_y, 2n_z$ shown in Fig(2.1). The directions in the crystal along are the directions where **D** and **E** are parallel. The ellipsoid is known as the *index ellipsoid* or *optical indicatrix*.

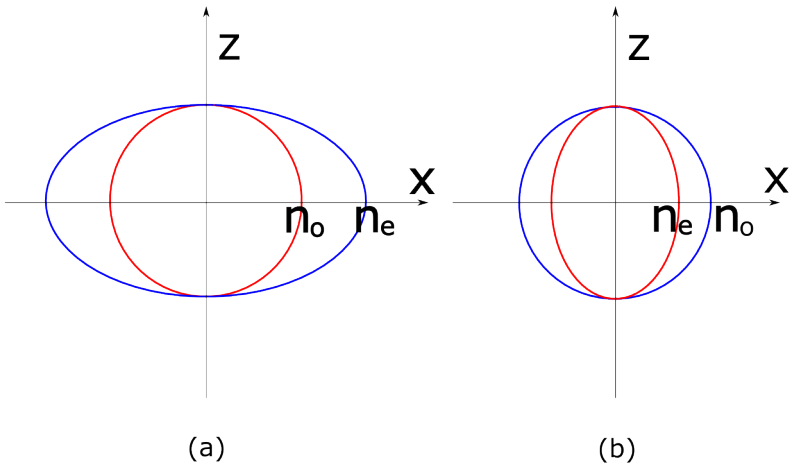

Figure 2.2: Intersection of the normal surface with the xz plane for (a) positive uniaxial crystal, (b) negative uniaxial crystal.

Uniaxial Crystals

In uniaxial crystals which the highest degree of rotational symmetry applies to no more than a single axis, (2.12) simplifies to

$$\frac{x^2}{n_o^2} + \frac{y^2}{n_o^2} + \frac{z^2}{n_e^2} = 1 \tag{2.13}$$

where the axis of symmetry was chosen, as the z axis. It is referred as optical axis, n_o is called the ordinary index of refraction and n_e is the extraordinary index of refraction[1]. As shown in Fig(2.2), if $n_e < n_o$, the crystal is referred as negative uniaxial crystal, whereas in a positive uniaxial crystal, $n_e > n_o$. The existence of an ordinary and an extraordinary ray with different indices of refraction is called birefringence.

[1]Since the crystal used in this experiment is an uniaxial crystal, the uniaxial crystal will be emphasized here rather than the biaxial crystal where it contains two optical axes.

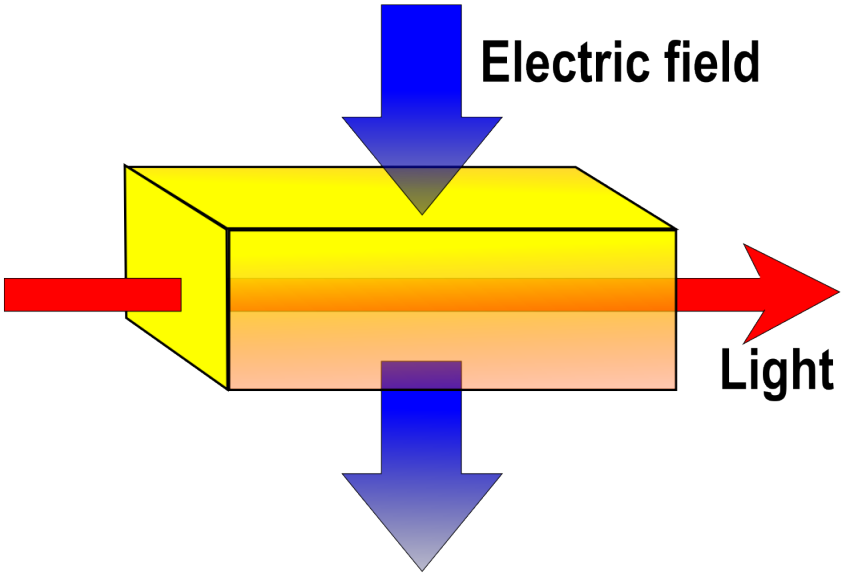

Figure 2.3: An electric field applied to an electro optic material modifies its refractive indices. The electric field therefore modulates the light passing through this electro optic material.

2.2 Electro Optics

Electro optic effect is an effect when an electric field is applied to a crystal, the ionic constituents move to new locations determined by the field strength and the restoring force. A field applied to an anisotropic electro optic material modifies its refractive indices and thereby its effect on polarized light as shown in Fig(2.3). Anisotropy in the optical properties therefore can be due to the unequal restoring force along three mutually perpendicular axes in the crystal. These changes can be described in terms of the modification of the index ellipsoid.

The linear electro optic effect or Pockel effect is the change in the indices of the ordinary and extraordinary rays is proportional to an applied electric field. This effect exists only in crystals that do not possess inversion symmetry[2].

[2]A crystal contains a regular lattice of points such that inversion about any one of these points leaves

The propagation characteristics in crystals are described by the index ellipsoid (2.12). Consider the equation of index ellipsoid in the presence of an electric field as

$$\left(\frac{1}{n^2}\right)_1 x^2 + \left(\frac{1}{n^2}\right)_2 y^2 + \left(\frac{1}{n^2}\right)_3 z^2 + 2\left(\frac{1}{n^2}\right)_4 yz + 2\left(\frac{1}{n^2}\right)_5 xz + 2\left(\frac{1}{n^2}\right)_6 xy = 1 \tag{2.14}$$

With zero electric field, (2.14) reduces to (2.12), meaning that

$$\left(\frac{1}{n^2}\right)_1\Big|_{E=0} = \frac{1}{n_x^2} \tag{2.15}$$

$$\left(\frac{1}{n^2}\right)_2\Big|_{E=0} = \frac{1}{n_y^2} \tag{2.16}$$

$$\left(\frac{1}{n^2}\right)_3\Big|_{E=0} = \frac{1}{n_z^2} \tag{2.17}$$

$$\left(\frac{1}{n^2}\right)_4\Big|_{E=0} = 0 \tag{2.18}$$

$$\left(\frac{1}{n^2}\right)_5\Big|_{E=0} = 0 \tag{2.19}$$

$$\left(\frac{1}{n^2}\right)_6\Big|_{E=0} = 0 \tag{2.20}$$

The linear change in the coefficients due to an electric field is defined by

$$\Delta\left(\frac{1}{n^2}\right)_i = \sum_{j=1}^{3} \mathbf{r}_{ij} E_j \tag{2.21}$$

where in the summation over j, $1 = x$, $2 = y$, $3 = z$. This can be expressed in a matrix form as

$$\begin{pmatrix} \Delta\left(\frac{1}{n^2}\right)_1 \\ \Delta\left(\frac{1}{n^2}\right)_2 \\ \Delta\left(\frac{1}{n^2}\right)_3 \\ \Delta\left(\frac{1}{n^2}\right)_4 \\ \Delta\left(\frac{1}{n^2}\right)_5 \\ \Delta\left(\frac{1}{n^2}\right)_6 \end{pmatrix} = \begin{pmatrix} \mathbf{r}_{11} & \mathbf{r}_{12} & \mathbf{r}_{13} \\ \mathbf{r}_{21} & \mathbf{r}_{22} & \mathbf{r}_{23} \\ \mathbf{r}_{31} & \mathbf{r}_{32} & \mathbf{r}_{33} \\ \mathbf{r}_{41} & \mathbf{r}_{42} & \mathbf{r}_{43} \\ \mathbf{r}_{51} & \mathbf{r}_{52} & \mathbf{r}_{53} \\ \mathbf{r}_{61} & \mathbf{r}_{62} & \mathbf{r}_{63} \end{pmatrix} \begin{pmatrix} E_1 \\ E_2 \\ E_3 \end{pmatrix}$$

the crystal structure invariant.

The 6×3 matrix with elements $\mathbf{r}_{ij}$ is called the electro optic tensor. The matrix form describes electro optic tensor depends on the symmetry of the crystal and is related to the symmetry of the piezoelectric tensor[3].

In the next section, the electro optic effect of a particular crystal, Lithium Niobate will be studied using the general expressions mentioned above.

2.2.1 Lithium Niobate

There is a very large variety of useful electro optic materials, covering a wide range values for the electro optic tensors, refractive indices, response time and etc. However, most commercial devices use crystals for example, Potassium Dihydrogen Phosphate (KH_2PO_4) also known as (KDP), Barium Tantalate ($BaTiO_3$), Lithium Tantalate ($LiTaO_3$), Lithium Niobate ($LiNbO_3$) and some liquid crystals.

Since the first fabrication of indiffused waveguides in Lithium Niobate in 1974[5], this material has been extensively used for integrated photonics research. The Lithium Niobate has excellent optical and electro optical properties[6] and is capable of a high speed response. The treatment of the electro optic effect of Lithium Niobate is largely based on [7], with appropriate additions. It is interesting to note that the development in the Lithium Niobate area has been rapid since the writing of this paper late in 1987.

[3]Piezoelectric is the phenomenon in which the electric force causes a voltage to develop between the faces of the crystal. The voltage appears is due to the force has caused polarization.

The electro-optic tensor for a Y cut Lithium Niobate ($LiNbO_3$) in this experiment is[8][9]

$$\begin{pmatrix} 0 & -\mathbf{r}_{22} & \mathbf{r}_{13} \\ 0 & \mathbf{r}_{22} & \mathbf{r}_{13} \\ 0 & 0 & \mathbf{r}_{33} \\ 0 & \mathbf{r}_{51} & 0 \\ \mathbf{r}_{51} & 0 & 0 \\ -\mathbf{r}_{22} & 0 & 0 \end{pmatrix}$$

where $\mathbf{r}_{33} = 30.8$, $\mathbf{r}_{13} = 8.6$, $\mathbf{r}_{22} = 3.4$, $\mathbf{r}_{42} = 28$ in units of 10^{-12}m/V whereas the refraction indices are $n_e = 2.200$ and $n_o = 2.286$. Since $n_e < n_o$, the crystal is a negative uniaxial crystal.

It follows that, from the matrix form

$$\Delta\left(\frac{1}{n^2}\right)_1 = -\mathbf{r}_{22}E_y + \mathbf{r}_{13}E_z \tag{2.22}$$

$$\Delta\left(\frac{1}{n^2}\right)_2 = \mathbf{r}_{12}E_y + \mathbf{r}_{13}E_z \tag{2.23}$$

$$\Delta\left(\frac{1}{n^2}\right)_3 = \mathbf{r}_{33}E_z \tag{2.24}$$

$$\Delta\left(\frac{1}{n^2}\right)_4 = \mathbf{r}_{51}E_y \tag{2.25}$$

$$\Delta\left(\frac{1}{n^2}\right)_5 = \mathbf{r}_{51}E_x \tag{2.26}$$

$$\Delta\left(\frac{1}{n^2}\right)_6 = -\mathbf{r}_{22}E_x \tag{2.27}$$

In the experiment discussed in this project, the applied external electric field is along z direction and zero in x and y directions. The matrix form can be simplified becomes

$$\Delta\left(\frac{1}{n^2}\right)_1 = \mathbf{r}_{13}E_z \tag{2.28}$$

$$\Delta\left(\frac{1}{n^2}\right)_2 = \mathbf{r}_{13}E_z \tag{2.29}$$

$$\Delta\left(\frac{1}{n^2}\right)_3 = \mathbf{r}_{33}E_z \tag{2.30}$$

Using (2.14), the following equation of the index ellipsoid in the presence of E_z can be obtained

$$\underbrace{\left(\frac{1}{n_o^2}+\mathbf{r}_{13}E_z\right)}_{\frac{1}{n_x^2}}x^2+\underbrace{\left(\frac{1}{n_o^2}+\mathbf{r}_{13}E_z\right)}_{\frac{1}{n_y^2}}y^2+\underbrace{\left(\frac{1}{n_e^2}+\mathbf{r}_{33}E_z\right)}_{\frac{1}{n_z^2}}z^2 \;=\; 1 \tag{2.31}$$

Since no mixed terms appear in (2.31), the principal axes of the new index ellipsoid remain unchanged[4].

Assuming $\mathbf{r}_{13}E_z \ll n_o^{-2}$ and $\mathbf{r}_{33}E_z \ll n_e^{-2}$. The refractive indices x, y and z axis are

$$n_x \;=\; n_o-\frac{1}{2}n_o^3\mathbf{r}_{13}E_z \tag{2.32}$$

$$n_y \;=\; n_o-\frac{1}{2}n_o^3\mathbf{r}_{13}E_z \tag{2.33}$$

$$n_z \;=\; n_e-\frac{1}{2}n_e^3\mathbf{r}_{33}E_z \tag{2.34}$$

In short, when an electric field is directed along the optic axis or z axis of Lithium Niobate, this crystal remains uniaxial with the same principal axes, but its refractive indices are modified in accordance with (2.32), (2.33) and (2.34). Fig(2.4) shows how does the index of ellipsoid changes when the external electric field is applied in z direction[10]. Since the change of the refractive indices along the principal axes are not the same, this will result different light modulation on a light which polarized in different directions. Meaning that, the effect of a light modulation is polarization dependent.

[4]For example, if the electric field is in y direction, the modified index ellipsoid contains a cross term in yz and thus the original principal axes are no longer appropriate. A new set of principal axes has to be defined to eliminate the cross term.

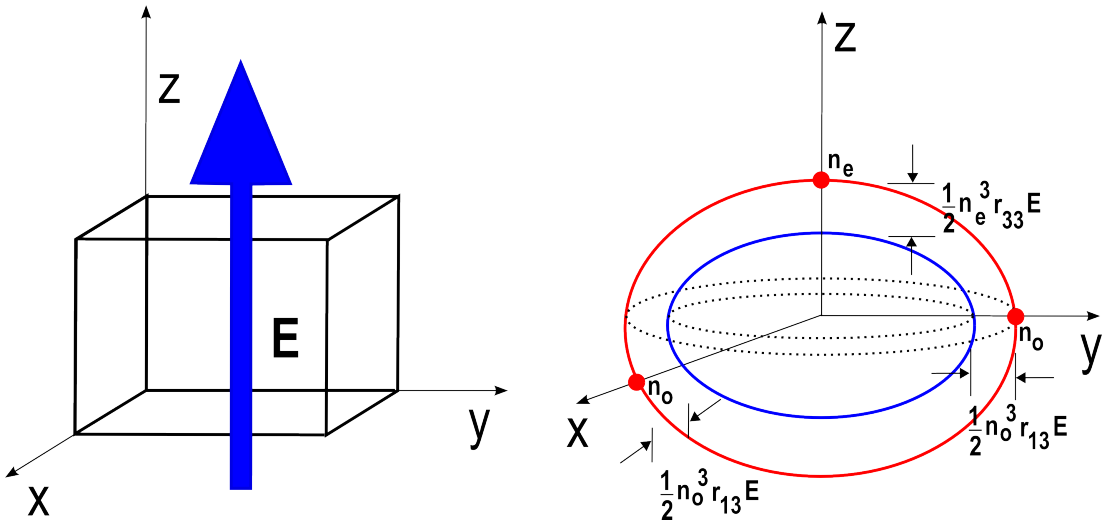

Figure 2.4: Modification of the index ellipsoid of a Lithium Niobate crystal caused by an electric field in the direction of the optical axis. The red ellipse is the index ellipsoid of the crystal without electric field. The blue ellipse is the index ellipsoid after the electric field is applied in z direction.

2.3 Configurations of Electro Optic Modulator

Since Dr. Kaminow & his team members from Bell Labs reported the concept of electro optic light modulator[11] using the electro optic effect, the research and development in this technology has produced tremendous improvement in device characteristics. By modifying the refractive index of a material, electro optics provides the means to alter the amplitude, phase and direction of a light beam. In this project, a device is built to use this modification of refractive indices to modulate the phase of the light as shown in Fig(2.5). The device is a bulk modulator, although many of them are more efficiently operated in waveguide or integrated optics technologies (because of the advantages of miniaturization), they are still needed for bulk optics applications since they are not as lossy as integrated optical elements.

In general, there are two configurations to set up the phase modulator, longitudinal mode

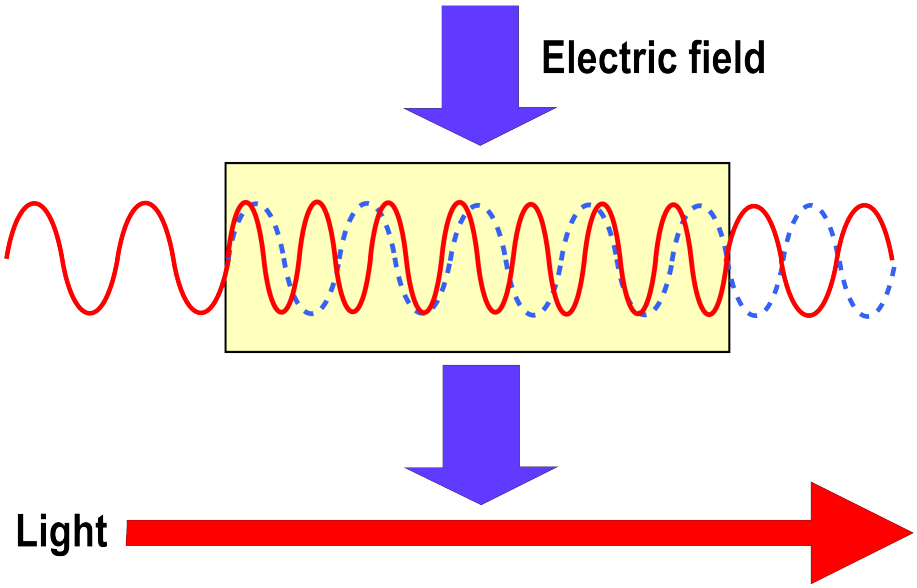

Figure 2.5: Phase modulator modulates the travelling light wave. The dashed line indicates the light wave without passing through the crystal.

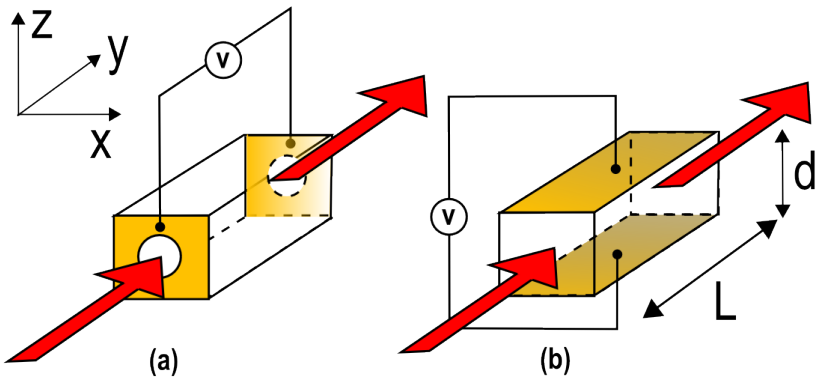

Figure 2.6: (a) Longitudinal modulator. The electrodes are placed in both ends of the crystal. (b) Transverse modulator. The electrodes are placed on the top and the bottom of the crystal.

and transverse mode of operation as shown in Fig(2.6). In the longitudinal mode operation, the applied external electric field is along the direction of propagation of the beam. The phase shift is independent of the length of the crystal and depends only on applied electric field. Furthermore, this mode of operation needs transparent electrodes with a small aperture at the centre of the electrodes on both ends through which the beam can pass through.

The transverse electro optic modulator is the modulating electric field is perpendicular to the optical beam path. This structure provides a long interaction length at a given field strength and the field electrodes do not interfere with the optical beam. The phase shift is proportional to the ratio of the width of the crystal to its length. Thus by decreasing this ratio, the applied voltage or electric field can be greatly reduced.

2.3.1 Phase Modulator

In the project discussed here, a transverse mode modulator is preferred. Since the electric field is applied in z direction and the the light beam is propagating in y direction, from (2.34) and (2.32), the birefringence seen by the light is

$$\begin{aligned} \Delta n &= n_z - n_x \\ &= n_e - n_o - \frac{1}{2}(n_e^3 \mathbf{r}_{33} - n_o^3 \mathbf{r}_{13})E \end{aligned} \tag{2.35}$$

For a incoming light polarized in z direction, the phase shift induced by the crystal is

$$\begin{aligned} \Delta\phi &= \frac{2\pi L}{\lambda}(n_z - n_e) \\ &= \frac{2\pi L}{\lambda}(\frac{1}{2}\mathbf{r}_{33} n_e^3 E_z) \end{aligned} \tag{2.36}$$

where λ is the wavelength of the light, L is the crystal length and d is the crystal thickness (refer to Fig(2.6)).

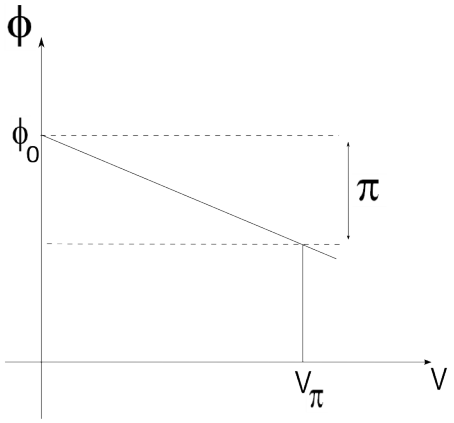

Figure 2.7: A graph illustrates the phase shift after the crystal is being applied an electric field or voltage.

Since $E_z = \frac{V}{d}$, the voltage required to induce $\Delta\phi$ phase shift is

$$V_z = \frac{\lambda d \Delta\phi}{\pi L \mathbf{r}_{33} n_e^3} \tag{2.37}$$

Generally speaking, the overall phase shift, ϕ is shown in Fig(2.7) and the equation is given as

$$\begin{aligned} \phi &= \phi_0 - \Delta\phi \\ &= \phi_0 - \pi \frac{V_z}{V_\pi} \end{aligned} \tag{2.38}$$

where $\phi_0 = \frac{2\pi n L}{\lambda}$. It is common practice to characterize the crystal by a half wave voltage, V_π, which is the voltage required to induce a phase shift of π. The half wave voltage for light polarized in z direction is

$$V_{\pi,z} = \frac{\lambda d}{L \mathbf{r}_{33} n_e^3} \tag{2.39}$$

However, for an incoming light polarized in x direction, the phase shift induced by the crystal is

$$\Delta\phi = \frac{2\pi L}{\lambda}(n_x - n_o)$$

$$= \frac{2\pi L}{\lambda}(\frac{1}{2}\mathbf{r}_{13}n_o^3E_z) \tag{2.40}$$

It can be shown that the half wave voltage for light polarized in x direction is

$$V_{\pi,x} = \frac{\lambda d}{L\mathbf{r}_{13}n_o^3} \tag{2.41}$$

From (2.39) and (2.41), $V_{\pi,x}$ is 3.2 times larger than $V_{\pi,z}$. This results is reasonable since the modulating electric field is parallel to the z polarized light. Hence, the experiment setup should prepare the incoming light polarized in z direction since it requires lower voltage[5]. The table below shows some typical half wave voltages for different wavelengths and polarizations.

Lithium Niobate : length of 2cm & thickness of 1mm		
λ/nm	Polarization	V_π
633	z direction	97V
	x direction	308V
690	z direction	105V
	x direction	336V

In short, the electric field pointed in z direction does not introduce new principal axes such that the phase modulator can accept the light polarized in either x or z direction. On the other hand, if the electric field pointed in x or y direction, it will cause a little trouble since the phase modulator only accepts the light polarized in new principal axes where the axes have to be identified in advanced.

[5]Light polarized other than these two directions will not be discussed here since the amplitude of the outcoming light is also modulated rather than just only the phase. In this mode, the modulator is considered as an electronically tunable waveplate

Clearly, how much phase shift induced by certain applied voltage depends on the polarization of the incoming light. A graph shown in Fig(2.8) is a comparison of half wave voltages with different types of same dimensional crystals. A polarization independent phase shifter shall work for whatever polarization and it still induces the same amount of phase shift. The setup of a polarization-independent phase shifter will be discussed in the next chapter.

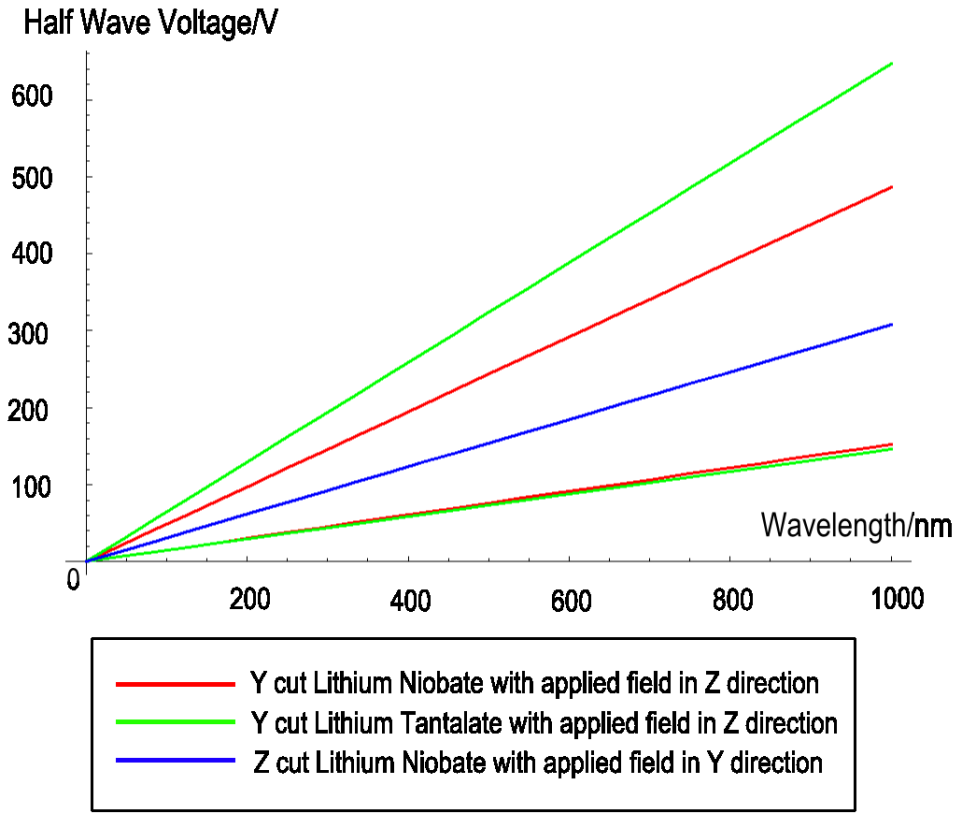

Figure 2.8: Half wave voltage of Lithium Niobate and Lithium Tantalate crystals. The dimensions of the crystals are the same for the voltage comparison. For Y cut Lithium Niobate and Lithium Tantalate crystals, they can accept either one of the two orthogonal polarizations as mentioned. However, for a Z cut Lithium Niobate crystal, the principal axes change with the voltage and therefore is not very useful for phase modulation.

Chapter 3

Experimental Setup

The polarization independent phase shifter in this project is based on the general electro optic modulator discussed previously. However, further improvements have been done by inserting a few optical elements to fix the polarization before it enters the crystal regardless whatever polarizations of light sent into the modulator. In this chapter, the experimental setup will be discussed and this gives a clear picture of the experimental setup working principles.

3.1 Polarization Independent Phase Shifter Setup

The laser source in this experiment were a 633nm Helium Neon gas laser and a 690nm laser diode (Hitachi HL6738MG). The lasers were coupled into a single mode fiber where the focus of the laser beam can be adjusted by placing an aspheric lens on the another end of the fiber.

As shown in Fig(3.1), the setup is a triangle loop where any incoming polarization light will be polarized by a $1cm^3$ polarizing beam splitter cube (PBS) before entering the loop. The PBS splits the light into two paths where their polarizations are orthogonal to each

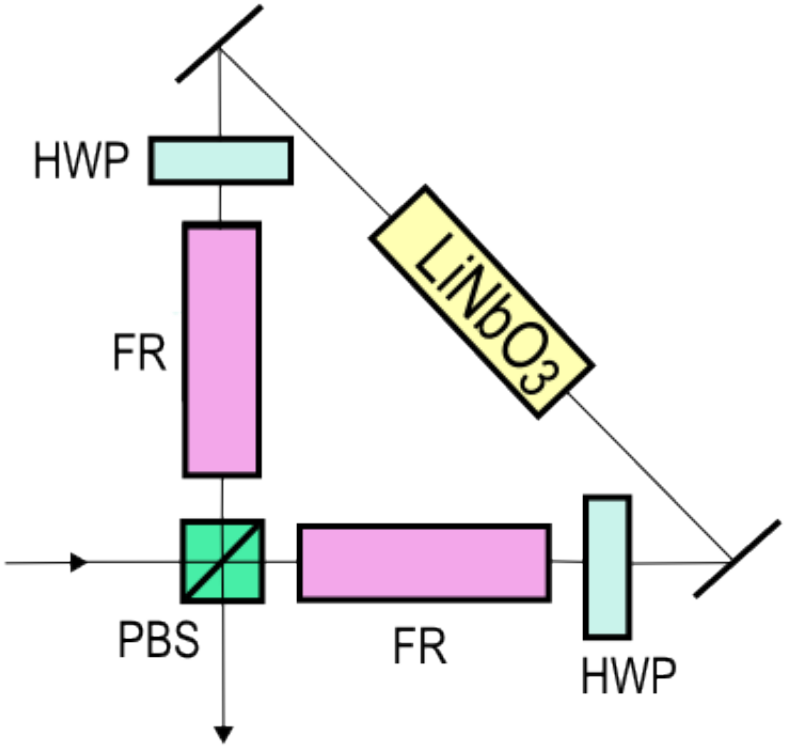

Figure 3.1: Schematic diagram of a polarization independent phase shifter.

other, horizontal polarization is transmitted and vertical polarization is reflected. These two polarization lights will be counter propagating in the triangle loop.

The Faraday rotators (FR) were set to rotate the incoming polarization by anti clockwise 45 degrees. Two half wave plates (HWP) where the fast axes are set at 67.5 degree and 112.5 degrees and placed in the transmitted arm and reflected arm respectively. With the Faraday rotators and waveplates setup in this experiment[1], incoming light polarized in horizontal or vertical direction will be changed to the same polarized direction (in our case, the preferred direction is horizontal polarization (90 degrees polarization) since the voltage required to induce the phase shift is much lesser) before they enter the crystal. Eventually, the two

[1]For Faraday rotator, the sense of polarization rotation is invariant to the direction of travel of the optical beam.

counter propagating beams acquire the same amount of phase shift. Ideally, the two beams will recombine and recover to the same initial state of polarization with a overall phase shift. This scheme works for any polarization light since any linearly polarized light can be decomposed into two orthogonal polarizations, vertical and horizontal. Fig(3.2) and (3.3) show the changes of polarization state when the light travels in each optical component.

3.1.1 Waist Scan Measurements

The dimension of the Lithium Niobate crystal is 1mm×1mm×2cm where it allows the light to propagate in this 2cm long crystal. Since the area of incidence is only 1mm×1mm, the laser was focused down to a waist of only 90μm. Waist measurements were done by monitoring the intensity collected by a photodetector, at the same time, the razor blade mounted on a motorized stage is blocking the laser light getting into photodetector in a step of 0.01mm, see Fig(3.4). Since the intensity profile is a Gaussian profile, the measurement can be fitted with certain function and hence the beam size can be determined. Waist measurement were done in several places to determine the focus point (smallest beam size).

In the analysis of a transverse electro optic modulator, one assumes the width of the crystal and its length to be independent of one another. In actual practice, for a given crystal length, l the minimum value of the width, d permissible will be determined by the beam diffraction inside the crystal[12]. Consider a Gaussian beam passing through the crystal as shown in the Fig(3.5). The size of the beam at any plane at a distance z from the waist is

$$w(z) \quad = \quad w_0(1 + (\frac{\lambda'^2 z^2}{\pi^2 w_0^4}))^{\frac{1}{2}} \tag{3.1}$$

where w_0 is the waist size of the Gaussian beam and $\lambda'^2 = \frac{\lambda_0}{n}$ is the wavelength of the beam

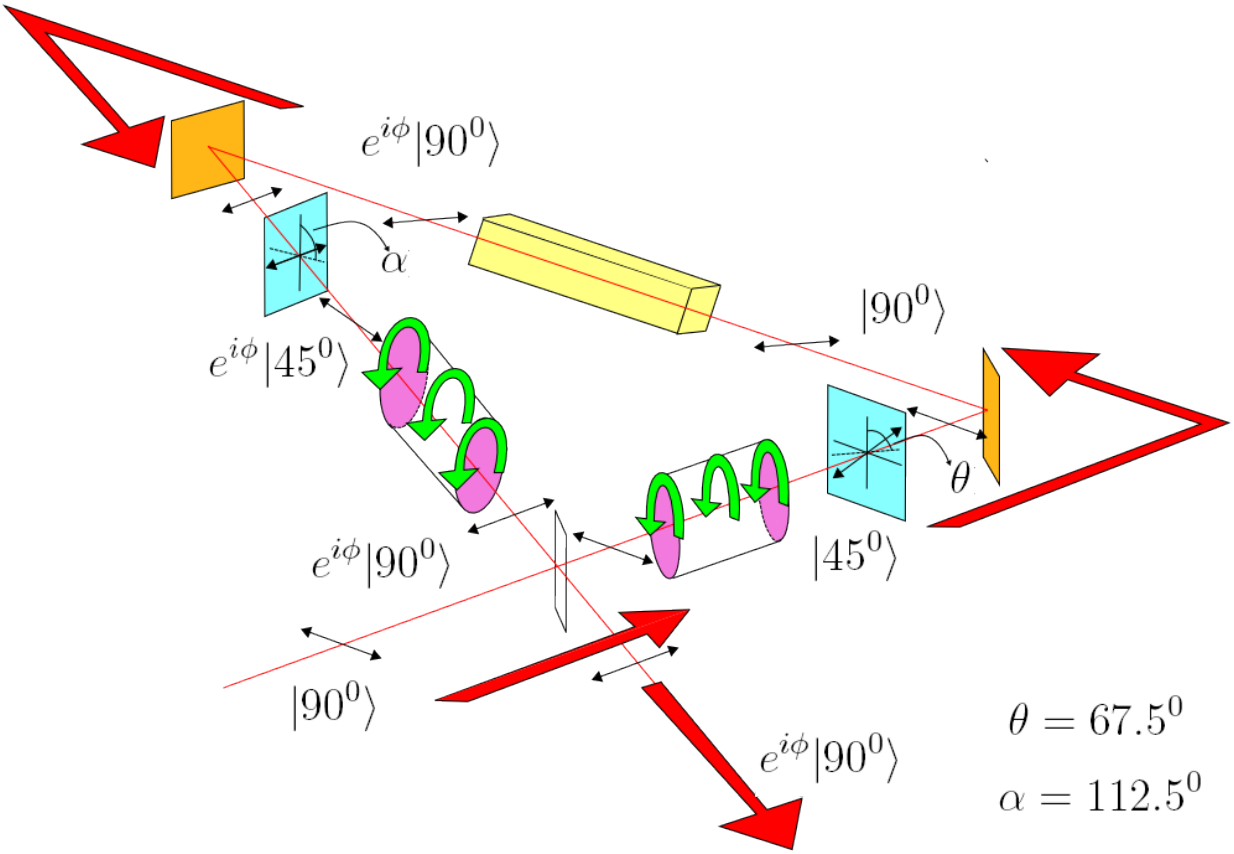

Figure 3.2: The diagram shows the horizontal polarization (90 degrees polarization) light is transmitted through the polarizing beam splitter (PBS). The light remains in the horizontal polarization before it enters the crystal. The light exits the loop remains horizontal polarization with a overall phase shift.

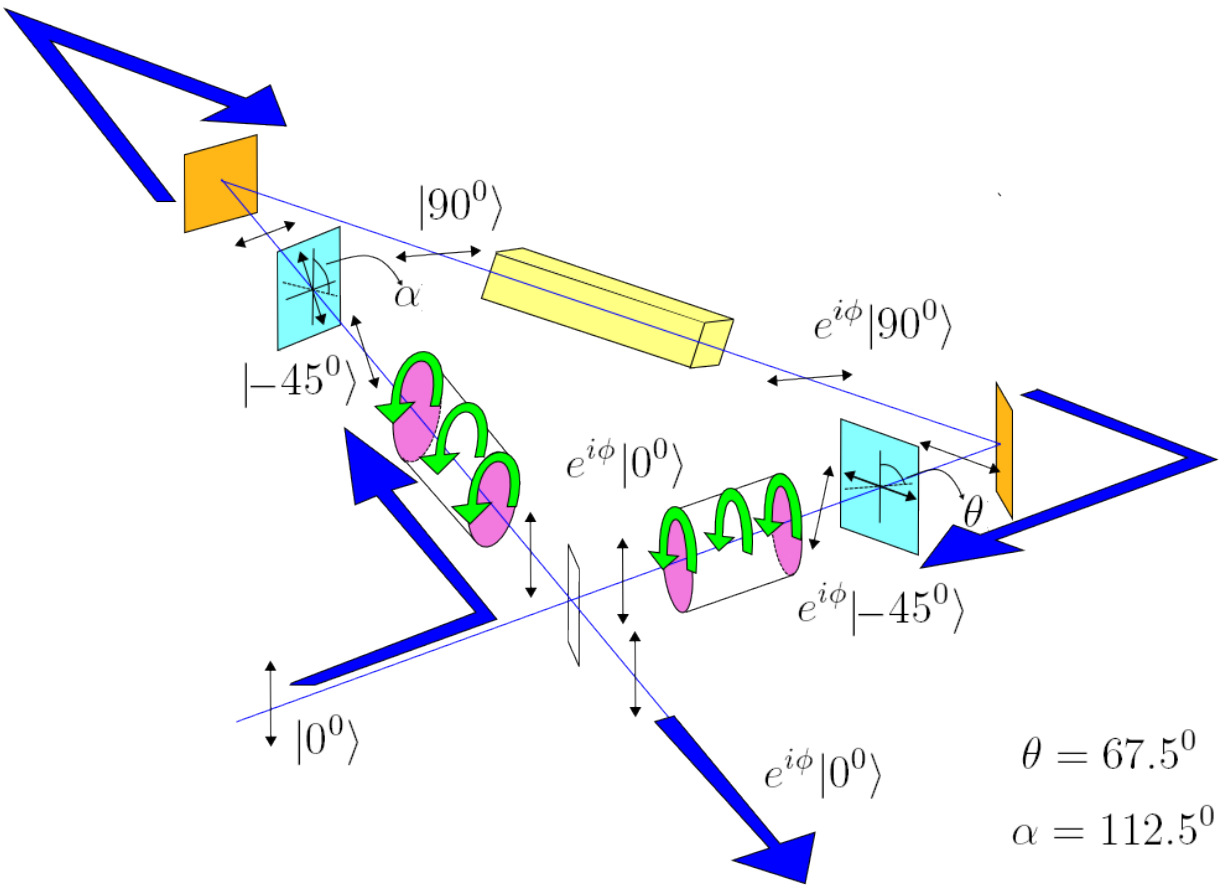

Figure 3.3: The diagram shows the vertical polarization (0 degree polarization)light is reflected at the polarizing beam splitter (PBS). The light has been changed to the horizontal polarization before it enters the crystal. The light exits the loop remains vertical polarization with a overall phase shift.

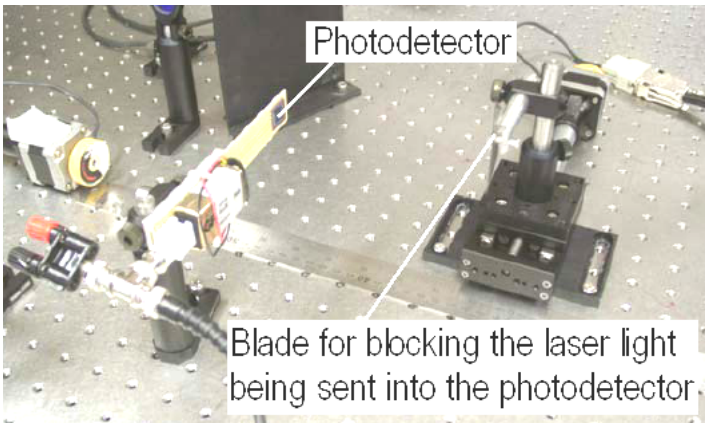

Figure 3.4: Beam size measurement.

in the medium with refractive index n. The diameter of the beam, D at the ends of the crystal is

$$\begin{aligned} D &= 2w(z = \frac{l}{2}) \\ &= 2w_0(1 + (\frac{\lambda'^2 l^2}{4\pi^2 w_0^4}))^{\frac{1}{2}} \end{aligned} \tag{3.2}$$

To find the optimum value of w_0 which gives the minimum D, set $\frac{d}{dw_0}(D) = 0$ and thus obtain $w_0 = \sqrt{\frac{\lambda' l}{2\pi}}$. Then by just substituting this w_0 into (3.1), the minimum D is

$$D = 2\sqrt{\frac{\lambda' l}{\pi}} \tag{3.3}$$

In the experiment discussed in this project, the $\lambda = 0.000690$mm, $l = 2$cm and $n = n_o \approx n_e$ and thus the minimum $D \approx 0.09$mm. However, the thickness or width of the crystal in this project is 1mm which implies the laser beam should be able to get into the crystal without being distorted.

By using the waist scan measurement, the beam waist in the air is found to be approximately 0.09 ± 0.01mm for the beam travels from the left and right towards the crystal. The separation of the two waists along the beam propagation direction is approximately

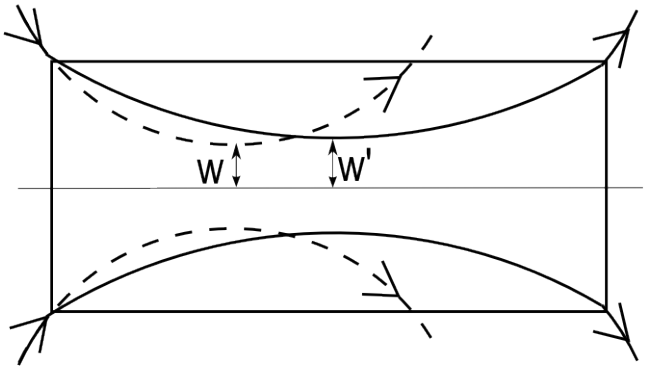

Figure 3.5: A Gaussian beam having a waist w in the air becomes w' when the light passes through the crystal. The diagram shows the optimum passage of the beam through a crystal. In the experiment, light travels from the left and right has to be positioned at the centre of the crystal.

(1.0±0.2)cm. When the crystal is put in the setup, both waists will be shifted to the centre of the crystal. Hence, the waist inside the crystal is , $w' = 0.13$mm and this gives the Rayleigh length, $z_R = \frac{\pi w'^2}{\lambda} = 8$cm which is long enough to cover the length of the crystal.

3.1.2 Aligning the Faraday Rotator

The Faraday rotator is an optical element where it tends to rotate the polarization of light in certain angles by sending the laser light through a crystal placed in a magnetic field. It is often referred as magneto optic effect. The rotator consisted of two 1.5cm long Terbium Gallium Garnet (TGG) crystals whereby the length exposed to the magnetic field determines the change of the polarization angle.

For the experiment discussed here, the rotator was set to rotate the polarization of light at the angle of 45 degrees. Fig(3.6) shows the laser light was polarized at 45 degrees before sending into the rotator. The laser was analyzed by a Glan-Taylor (GT) polarizing beam

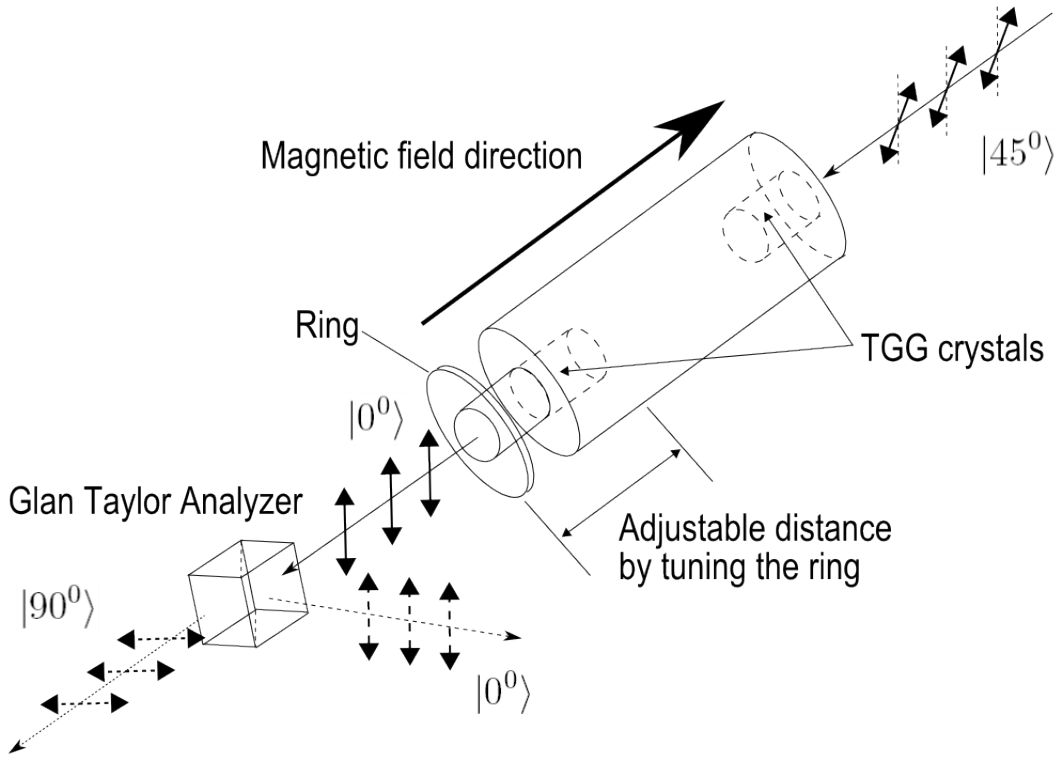

Figure 3.6: The Faraday rotator rotates the polarization angle using magneto optic effect. The TGG crystal was moved slowly until the light only exits in one of the two ports in the analyzer.

splitter after the rotator. A GT only allows the horizontal polarization (90 degrees) light to be transmitted while vertical polarization (0 degree) light will be reflected. Clearly, if the polarization angle is rotated either clock-wise or counter clock-wise 45 degrees, the light will only emit in transmitted or reflected port. The TGG crystal was displaced in and out of the rotator slowly until there is no light emitted in one of the ports. For the fine tuning, the rotator was reversed. Slowing tuning the ring until the light is totally emitted in another port. Now, the rotator had been properly aligned.

3.1.3 Aligning the Half Waveplate

A half waveplate is a birefringent crystal which allows to rotate the polarization of light. The refractive indices appear different for certain axes, if the polarization is not along with one of the principal axes, the polarization will be rotated after passes through the waveplate.

The half wave plates in this experiment rotate the polarization into horizontal polarization before the light enter the Lithium Niobate crystal. As shown in Fig(3.2) and Fig(3.3), the half wave plate in the transmitted arm was set at fast axis at 67.5 degrees and in the reflected arm at 112.5 degrees. The fast axis was determined by using the two Glan Taylor (GT) polarizing beam splitter. The first GT polarized the light in horizontal direction before sending the light into the waveplate. Then, the waveplate is rotated until the light only exits in the transmitted or reflected port of the second GT polarizing beam splitter. Together with the marking on the waveplate, the fast axis can be determined precisely.

3.1.4 Mounting the Lithium Niobate crystal

Fig(3.7) shows the crystal was attached to a circuit board with a high voltage across it. The board was mounted on a beam splitter mount for alignment purposes. The electrodes for the crystal are copper foils. In the later chapter, the circuit design of the board will be discussed in details.

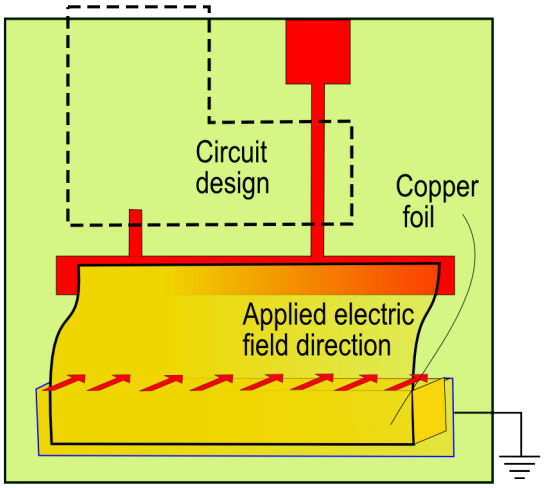

Figure 3.7: The Lithium Niobate crystal is in contact with the copper foils where the high voltage is able to be applied across the crystal. The circuit design inside the diagram will be discussed in the later chapter.

3.2 Phase Shift Measurement - Mach Zehnder Interferometer

The phase shift induced by the electro optic modulator is analyzed by a Mach Zehnder interferometer. The interferometer is an optical device which utilizes the effect of two beam interference, hence it is a sensitive tool to measure any phase shift between the two beams. By monitoring the intensity of the interference, the half wave voltage can be determined since the phase shift from 0 to π, the constructive interference undergoes to destructive interference or vice versa. In this chapter, we start with the brief review of a Mach Zehnder interferometer and some techniques for setting up a high visibility interferometer.

3.2.1 Brief Review of a Mach Zehnder Interferometer

A single photon always interferes only with itself as proposed by P.A.M. Dirac in 1932. The interpretation of the interference effects is different from classical experiments. The Mach Zehnder interferometer shown in Fig(3.8) is a good example to begin with. A photon prepared in $|\psi\rangle$ enters input 1 while input 2 is entered by the vacuum state $|0\rangle$. The initial state transforms to

$$|\psi\rangle_1 \longrightarrow \frac{1}{\sqrt{2}} i(|\psi\rangle_{1'} + ie^{i\phi}|\psi\rangle_{2'}) \tag{3.4}$$

before passing through the second beam splitter. The phase factor, i is due to the reflection on the mirror. Considering the second beam splitter into account, the transformation becomes

$$|\psi\rangle_1 \longrightarrow \frac{1}{2} i[(1 - e^{i\phi}|\psi\rangle_{1''}) + i(1 + e^{i\phi}|\psi\rangle_{2''})] \tag{3.5}$$

where the ϕ is the phase shift. Hence, the probability of finding a photon exit in the output $2''$ is

$$P_{2''} = |\langle\psi|_{2''}|\psi\rangle_1|^2 \tag{3.6}$$

$$= \cos^2(\frac{\phi}{2}) \tag{3.7}$$

Also the probability a photon exit in the output $1''$ is

$$P_{1''} = |\langle\psi|_{1''}|\psi\rangle_1|^2 \tag{3.8}$$

$$= \sin^2(\frac{\phi}{2}) \tag{3.9}$$

The graph illustrated in Fig(3.9) shows the probability of a photon (intensity) exit in these 2 outputs with respect to the phase shift. Clearly, the photon always exit in the output $2''$ if there is no phase shifter in between one of the arms. This is because the photon constructively interferes at output $2''$ and destructively interferes at output $1''$.

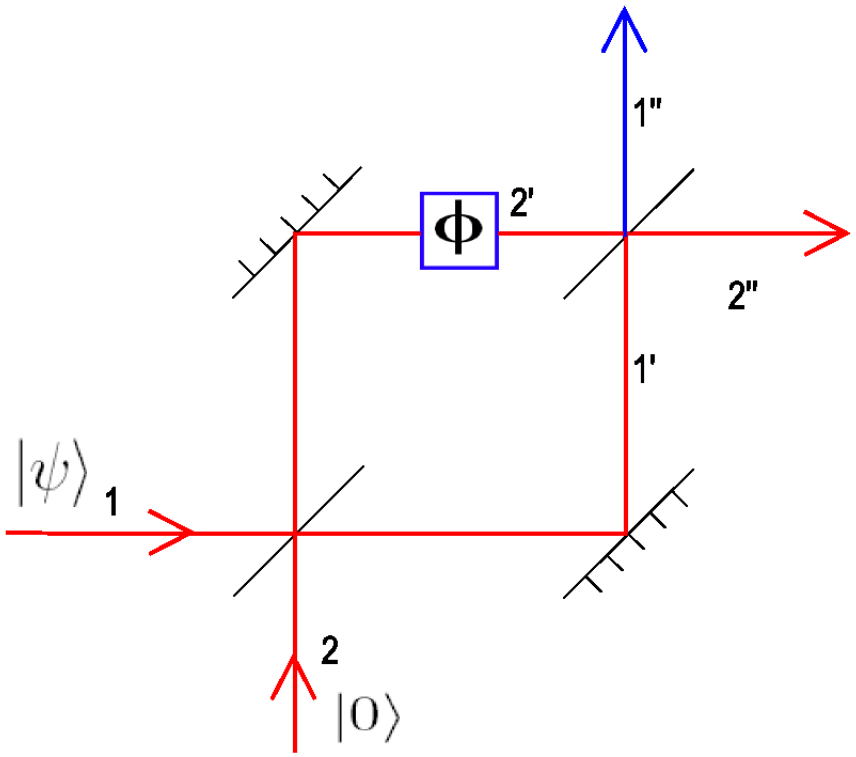

Figure 3.8: Mach Zehnder interferometer.

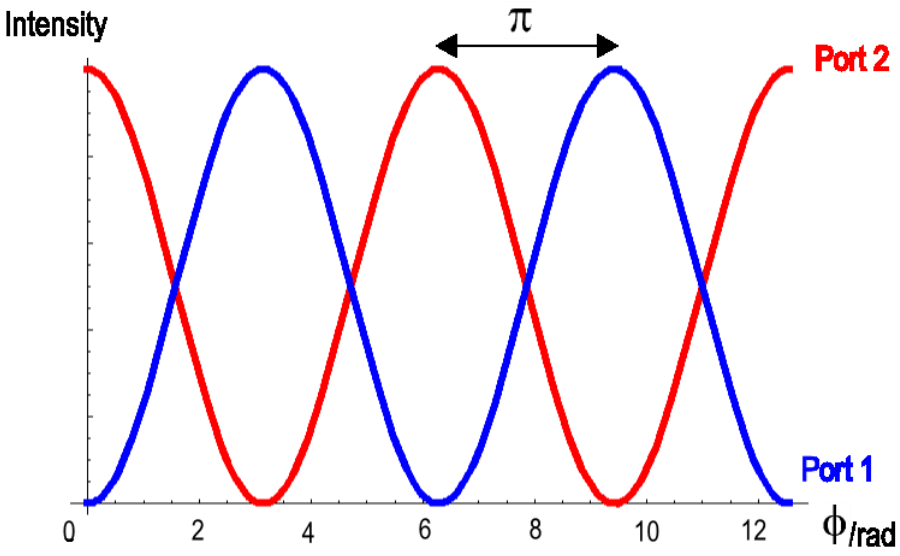

Figure 3.9: The phase shift can be determined by measuring the intensity at one of the two ports.

3.2.2 Condition For High Visibility Interference

Superposition principle is a basic property of all kinds of waves and is a key element to understand the condition for interference. When two waves are superimposed, the resulting amplitude distribution is the addition of the instantaneous amplitude of these two waves.

Consider an incident light beam with an electric field E which oscillates at a frequency ω and has travelled the path r

$$E = E_O e^{i(kr-\omega t)} \tag{3.10}$$

where E_O is the amplitude and k is the wave number equals to $\frac{2\pi}{\lambda}$. If the two beams from path A and B interfere with each other, the intensity is

$$I \propto |E_A + E_B|^2 \tag{3.11}$$

$$= E_{OA}^2 + E_{OB}^2 + E_{OA}E_{OB}(e^{ik(r_A-r_B)} + e^{-ik(r_A-r_B)}) \tag{3.12}$$

$$I = I_{OA} + I_{OB} + 2\sqrt{I_{OA}I_{OB}}\cos k(r_A - r_B) \tag{3.13}$$

Constructive interference corresponds to the cosine term equals to 1 whereas destructive interference is equals to -1. Hence,

$$I = \begin{cases} I_{max} = I_{OA} + I_{OB} + 2\sqrt{I_{OA}I_{OB}} & \text{for constructive interference} \\ I_{min} = I_{OA} + I_{OB} - 2\sqrt{I_{OA}I_{OB}} & \text{for destructive interference} \end{cases}$$

The visibility V is defined as follows

$$V = \frac{I_{max} - I_{min}}{I_{max} - I_{min}} \tag{3.14}$$

$$= \frac{2\sqrt{I_{OA}I_{OB}}}{I_{OA} + I_{OB}} \tag{3.15}$$

A full visibility V of 1 happens when $I_{min} = 0$. In general, the following conditions must be met for two waves to be interfered :

(1) *Same polarization.* Two waves with orthogonal polarization cannot interfere with each other.

(2) *Same frequency.* The two waves must oscillate at the same frequency to cancel the frequency dependent term in (3.12) as derived.

(3) *Constant phase relationship.* The phase difference must be constant at any given point in the superposition region. Otherwise, no stable interference pattern can be observed.

3.2.3 Interferometer Setup

Fig(3.10) shows a folded interferometer setup to measure the phase modulated by the Lithium Niobate crystal. The advantage of using a folded interferometer is the interferometer is relatively stable since only one beam splitter is needed. The laser beam is splitted into two paths using a 2.5cm^3 non-polarizing beam splitter cube (NPBS), one enters the triangle loop, and the other one is sent to the right angle mirror. Interference will be observed when the two beams recombine at the same NPBS again. Two aspects need to be considered in order to set up a high visibility interferometer : The *optical path length* and the *geometrical wavefront* from the two arms.

Optical Path Length

The interferometer built in this experiment is a symmetrical interferometer. Since the independent phase shifter setup contains certain optical elements with different refractive indices, the beam will travel extra optical path length. The extra optical path length, $L = (n-1)d$, where n is the refractive index of the optical element and d is the length of the optical element. The reason of building a symmetrical interferometer is because the coherence length of the testing laser (here a laser diode was used in this experiment) is too short. The coherence

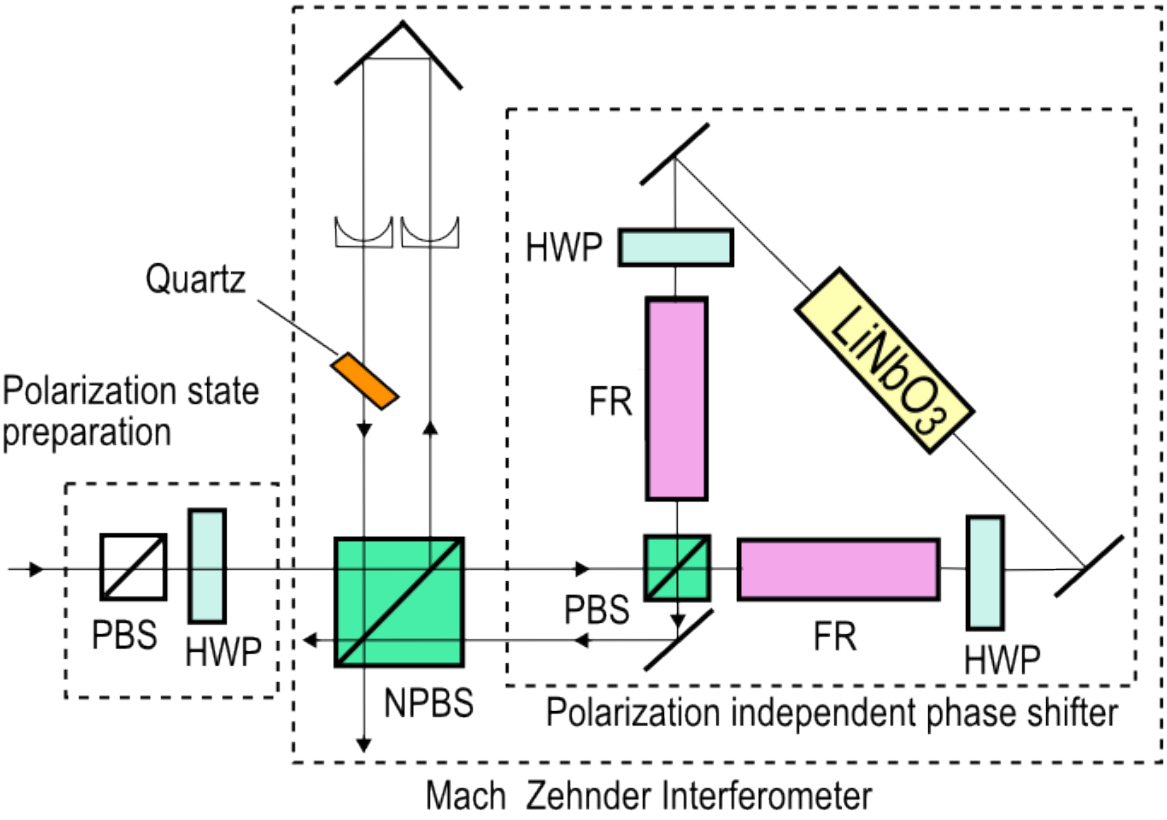

Figure 3.10: Complete experimental setup.

length measures how long the light waves remain in phase as they travel. The coherence length is very useful since it tells how far apart two points along the light beam can be but still remain coherent with each other. In interferometry, the coherence length is the maximum optical path length difference that can be tolerated between the two interfering beams.

The coherence length depends on the nominal wavelength and the spectral bandwidth of the laser beam, given as[13], $l_c = \frac{\lambda^2}{2\delta\lambda}$. For a typical inexpensive laser diode lasing at wavelength of 690nm and wavelength range of 1nm, the coherence length is only a few milimeter. If the interferometer built in this experiment is asymmetric with one arm is shorter or longer than a few milimeter, one should not expect interference pattern can be observed.

In the triangle loop, the light travels extra optical path length are

$$4d_{\mathrm{TGG}}(n_{\mathrm{TGG}} - 1) = 4 \times 1.5 \times (1.95 - 1) = 5.7\mathrm{cm}$$

$$d_{\mathrm{LiNbO_3}}(n_{\mathrm{LiNbO_3}} - 1) = 2 \times (2.2 - 1) = 2.4\mathrm{cm}$$

$$d_{\mathrm{PBS}}(n_{\mathrm{PBS}} - 1) = 1 \times (1.52 - 1) = 0.52\mathrm{cm}$$

where $n_{\mathrm{TGG}} = 1.95$, $n_{\mathrm{LiNbO_3}} = 2.2$, $n_{\mathrm{PBS}} = 1.52$ and $d_{\mathrm{TGG}} = 1.5\mathrm{cm}$, $d_{\mathrm{LiNbO_3}} = 2\mathrm{cm}$, $d_{\mathrm{PBS}} = 1\mathrm{cm}$. This implies the right angle mirror arm should displaced extra 8.6cm in addition to the geometrical length of the triangle loop (the distance where the beam leaves the NPBS and backs to the NPBS). See Fig(8.1) in Appendix for more information.

Geometrical Wavefront

In Fig(3.11), imagine the light origin is a point source, O, then O has an image in S at O_S and an image at O_2 in M2; O_S has an image O_{S1} in M1, and O_2 has an image O_{S2} in S.

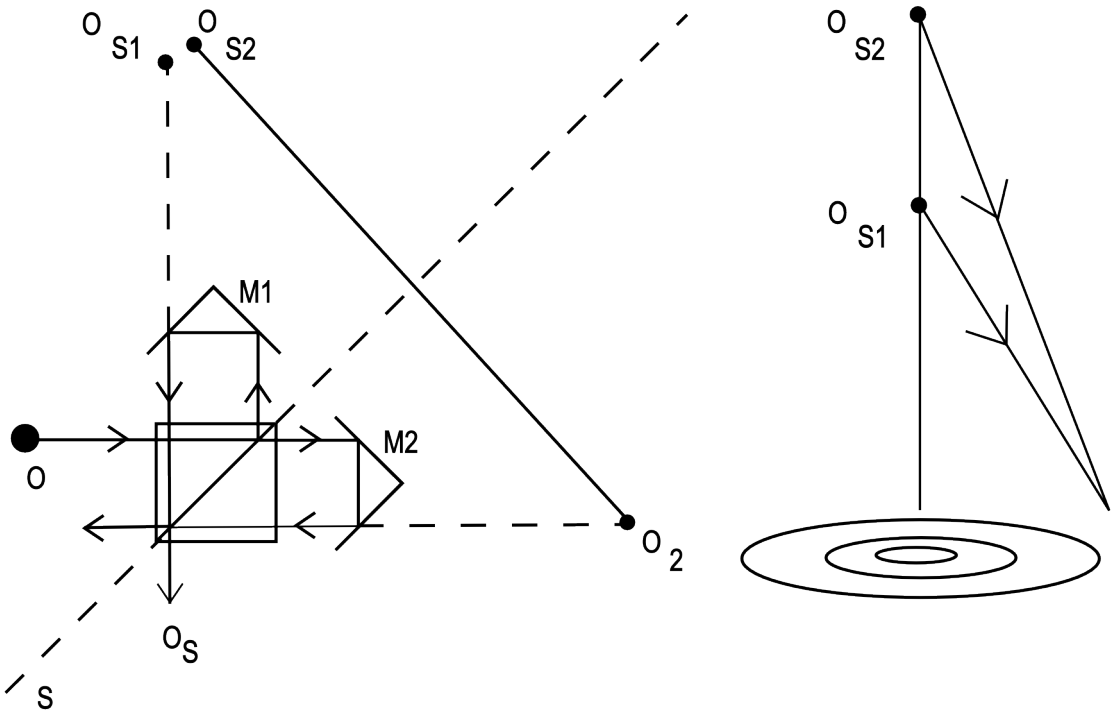

Figure 3.11: Two virtual sources give rise to interference. The right diagram shows the non-vanishing distance between these two sources produce circular fringes.

The images O_{S1} and O_{S2} are the two virtual sources that give rise to interference. In the experiment, O_{S1} and O_{S2} can be brought together by adjusting the length of one arm. The scale of the fringes depend upon the separation of these two virtual sources. If O_{S1} and O_{S2} are side by side, a set of straight fringes will be observed, the same situation as in Young's double slit experiment. The fringe separation gets wider as the two virtual points get closer.

In the Mach Zehnder interferometer, O_{S1} is placed in front of or behind O_{S2}. This leads to constructive or destructive interference on cones around the line joining O_{S1} and O_{S2}. The number of ring fringes is determined by the distance between these two virtual points. If the distance is zero, this corresponds to zero order interference with no dark fringes or a bright spot will be observed.

In the experiment, the mirror M1 was mounted on a translation stage for coarse movement and a piezo actuator inside for fine movement. The translation stage allows a movement of approximately 1cm and the piezo actuator allows a fine movement of several hundred micron. With the help of the translation stage, the mirror can be moved to the correct position, where the distance between O_{S1} and O_{S2} is zero. By applying an appropriate dc voltage to the piezo actuator (no more than 150V), the mirror could be further shifted until the observed interference only constructive or destructive interference.

3.2.4 Wavefront Correction

Since the length of the interferometer arm is fixed by the optical path length, both the wavefronts from the two beams could not match with each other perfectly when both beam return and meet at the NPBS. Since there is a length restriction due to the coherence length of the light as mentioned in section (3.2.3), the laser beam reflected at the NPBS has been focused down to certain position before it reaches the centre of the right angle mirror (due to the fact that length of the right angle mirror arm was extended and the laser beam transmitted at the NPBS has to be focused at the centre of the crystal). One way to shift the focus point to the centre of the right angle mirror would be placing a confocal setup in the arm using two concave lenses having the same focal length of 200mm (refer to Fig(3.10)). The confocal setup was moved along the arm until the visibility reaches maximum. The wavefront correction needs two concave lenses since they correct the focus of the beam and the beam size. One concave lens would not work since it only corrects the focus of the beam.

3.2.5 Phase Correction

Ideally, the non-polarizing beam splitter (NPBS) transmits or reflects whatever polarization of light by reducing half of the intensity and maintains the original polarization state.

However, practically, the beam splitter does not maintain the polarization state if the polarization neither horizontal nor vertical. As shown in Fig(3.12), if the incoming light consists of horizontal and vertical polarization keeping the fixed phase angle with each other[2], these two components do not necessary keep the same phase angle as previous after the light passes through the NPBS . This is because of the dielectric layer in the NPBS which acts differently for these two orthogonal polarizations. The light emitted becomes eventually elliptically polarized. As mentioned, only light with the same polarization gives a high visibility interference. Therefore, a quartz plate is necessary to compensate the unwanted phase shift due to the NPBS.

The phase correction is a key element to setup a laser light shutter with high extinction ratio. Without the compensation, an incoming light polarized neither horizontal nor vertical direction shows a very low visibility in this double pass interferometer. This is because two orthogonal polarizations do not interfere each other. One may see the horizontal polarization showing constructive interference, while the vertical polarization shows destructive interference. The low visibility gives an inaccurate half wave voltage measurement and a laser light shutter with low extinction ratio.

[2]Any linearly polarized light can be decomposed into two orthogonal polarization, where the polarization direction is respect to the plane of incidence. In electromagnetic theory, the two polarizations always referred to transverse magnetic wave, TM wave and transverse electric wave, TE wave.

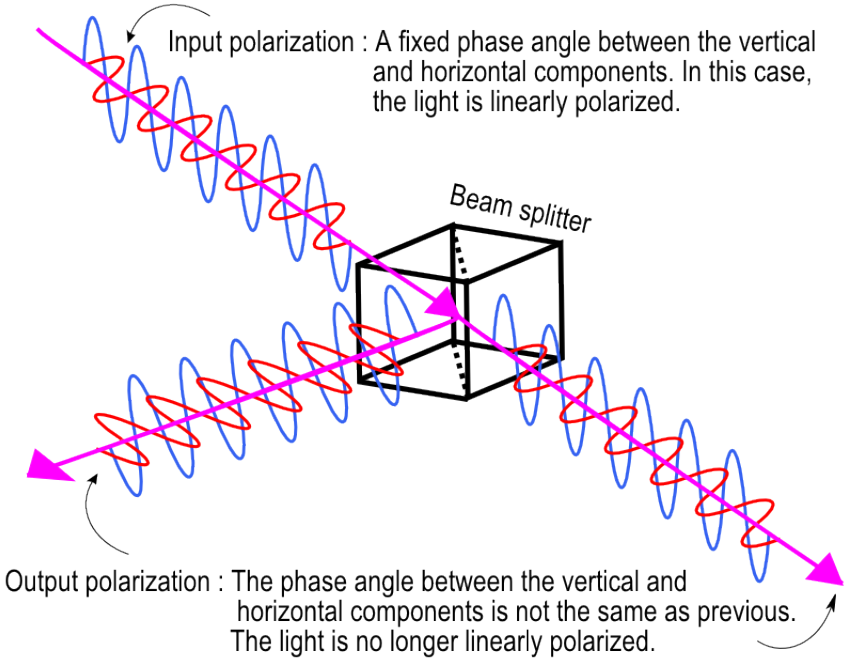

Figure 3.12: The beam splitter does not maintain the input polarization state due to the imperfection of the beam splitter.

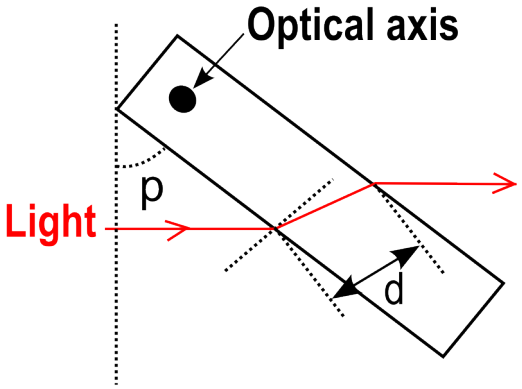

Figure 3.13: The optical axis of a quartz is pointed out of the paper towards the reader. By adjusting the angle θ, it effectively adjusts the distance d or the phase shift between the horizontal and vertical polarization components.

Aligning the Quartz Plate

To change the phase difference between these two orthogonal polarizations, one of the polarizations should be sent along the optical axis of the quartz plate. When the quartz plate is rotated around the optical axis as shown in Fig(3.13), it changes the optical path length, d. The two orthogonal polarizations travel at different speed because the refractive indices are different for these two polarizations. By adjusting the geometrical path length, the phase difference between these two polarizations can be chosen until it matches the polarization of the beam to be interfered.

The phase shift is given as

$$\delta\phi = \frac{2\pi d}{\lambda}(n_e - n_o) \tag{3.16}$$

where λ is the wavelength of the light in vacuum, d is the optical path length taken by the light travels inside the quartz, n_o and n_e. In the experiment, the angle θ was tilted until the visibility reached a maximum. Then, the phase correction is optimized.

Chapter 4

Practical Considerations

After discussing the electro optic material and the geometrical configurations of the modulator, there are some practical limitations which limit the performance of the modulator. General considerations are briefly reviewed in this chapter. The modulator is desirable to have[16]:

- High photorefractive damage threshold which enables the device to handle high optical power without the crystal being damaged.
- High optical transmission, low reflection, low scattering in the crystal.
- No distortions in the output of the modulator due to piezoelectric resonances.
- Low dielectric constant or a low capacitance enhances the response of the modulator (to be discussed in the next chapter).

4.1 Photorefractive Damage Threshold

Electro optic photoconductive materials present a very interesting phenomenon known as the photorefractive effect. This effect was discovered by Ashkin[17].

Mainly, the optical power handling capacity of electro optic crystal is limited by an effect known as photorefractive damage. This effect is related to the average optical power and is wavelength and intensity dependent. The photorefractive damage process can occur gradually over days or in the case of high optical powers or short wavelengths, in just a few seconds.

The damage is a result of photoexcited charge carriers migrating from illuminated regions to dark regions. This effect causes the local variations in the refractive index and then causes beam distortions[18]. Usually, magnesium oxide doped Lithium Niobate increases the damage threshold and this crystal are used in most of the commercial electro optic modulator. However, the drawback is the doped crystal increases the wavefront distortion as compared undoped Lithium Niobate. The damaged can be removed by heating the crystal slowly to about 50-70^{0}C, where the heat mobilizies the charge carriers. The damaged crystal can also be exposed to UV light to remove the photorefractive damage.

4.2 Optical Transmission

Since the Lithium Niobate crystal is 780nm anti-reflection coated, reflection from the end surfaces would be expected if other laser wavelength are used. A parameter named insertion loss, IL is defined to characterize the transmission of the optical beam inside the crystal.

The insertion loss is given as

$$IL = 10\log(\frac{I_1}{I_0}) \tag{4.1}$$

where I_1 is the maximum intensity after the light passes through the crystal and I_0 is the incident light intensity. The Y cut Lithiun Niobate crystal is 780nm anti-reflection coated, with the reflectance less than 0.25%. For a 633nm Helium Neon gas laser, the insertion loss was measured to be 20% or 1dB. This is because the 1.5cm long TGG crystals inside the Faraday rotators are not 633nm anti-reflection coated. Other than the reflection from the surface, a high optical transmission shows that there is less scattering inside the crystal. In fact, the longer the crystal is, the lower the half wave voltage is, but the insertion loss will be slightly higher. Since there is a finite transit time of the optical beam as it passes through the crystal, there will be some limitations on the frequencies of the modulating signal. Let τ be the time taken by the beam to pass through the crystal and is given by[12], $\tau = \frac{nl}{c}$. In earlier discussion, the phase shift expressions are derived after assuming the modulating electric field remains constant for the propagation time τ. In the experiment, the time $\tau = \frac{2.2\times2^{-2}}{3\times10^8} \approx 1.5 \times 10^{-10}s$. Therefore, if the modulating electric field is oscillating with a frequency of 7GHz, then the electric field no longer remains constant within the time taken by the beam to travel through the crystal. For the experiment discussed here, the transit time limitation is negligible.

4.3 Piezoelectric Effect

All electro optic crystals are piezoelectric. Therefore, sometimes the phase modulation can be accompanied by unwanted amplitude modulation and beam deflection. The reason is the electrical signal that produces the phase modulation also generates vibrations. The strains

induced by these vibrations alter the refractive indices by elasto optic effect. Hence, the crystal should not driven at a frequency where it induces the piezo resonance. Fortunately, the piezoelectric effect in Lithium Niobate is fairly weak and typically do not affect the performance of the crystal.

Chapter 5

High Frequency Modulator

The response of the modulator is limited by the geometrical configurations of the modulator and the time constant of the electrical circuit. Therefore, a proper electronic circuit design would enhance the quality of the modulator in terms of the speed it modulates the light with certain phase shift. In this chapter, the circuit aspect of the modulator will be discussed.

5.1 Electronic Circuit

Fig(5.1) is a electronic circuit built in this experiment. The main component is the BSS131 MOSFET or metal-oxide-semiconductor field-effect transistor that switches the voltage from half wave voltage to zero across the crystal. Negative pulses generated from the function generator (Agilent 33250A) are sent into a pulse shaper to further decrease the fall time. The fall time is the time required for the pulse to fall from 90% of the final value to 10% of the final value. As shown in Fig(5.3), the negative pulse after the pulse shaper has at least fall time 10 times shorter than the pulse without going through the pulse shaper.

These pulses will be sent into the gate of the MOSFET. In the normal operation[19], a

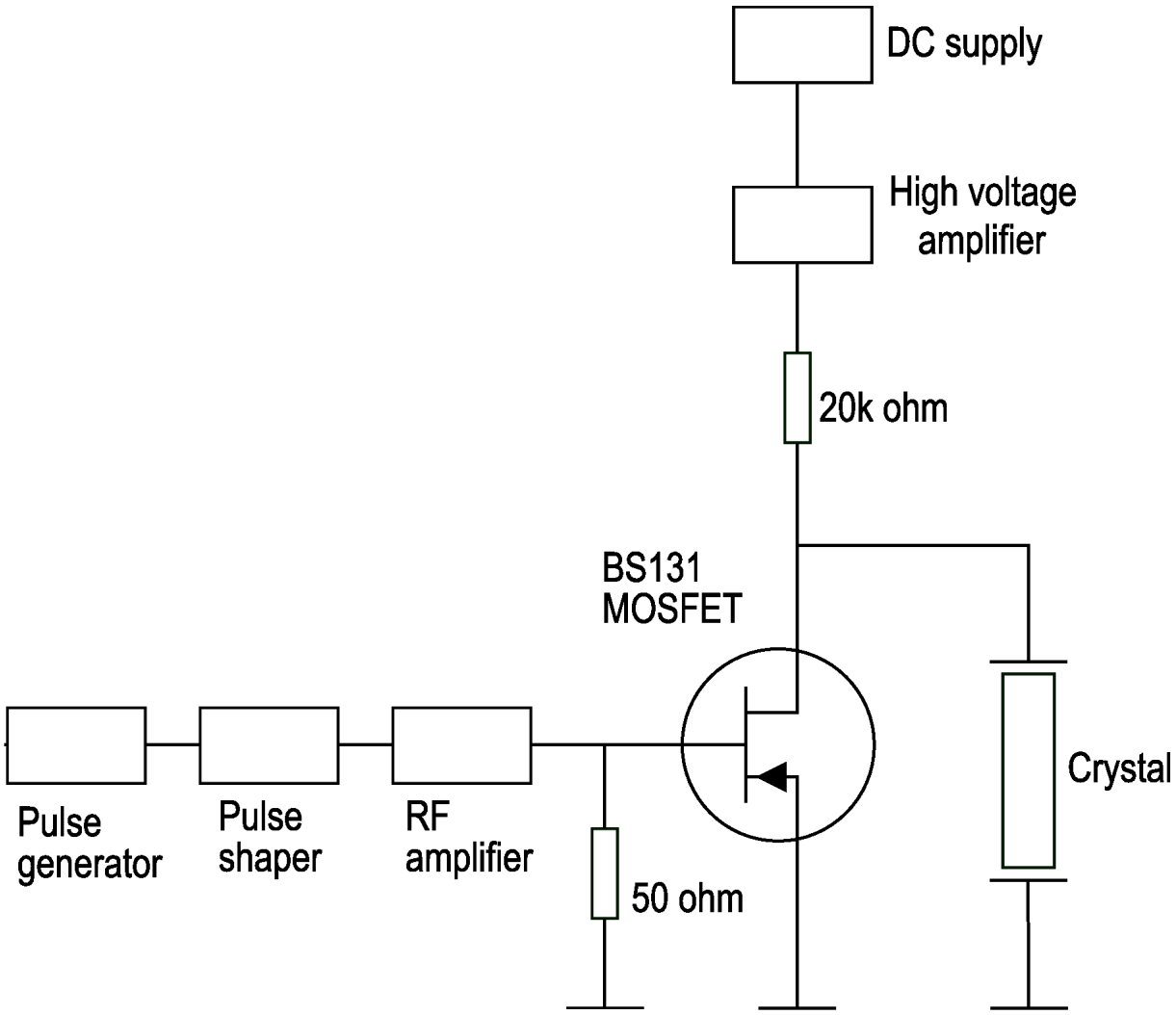

Figure 5.1: The circuit design of a switch.

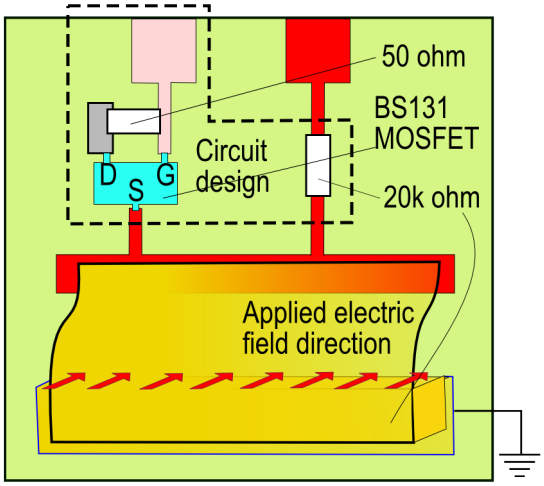

Figure 5.2: The diagram shows the crystal with the circuit on the circuit board. The drain (D) current flows when pulses are sent into the gate (G). A dc high voltage is constantly sent into the source (S).

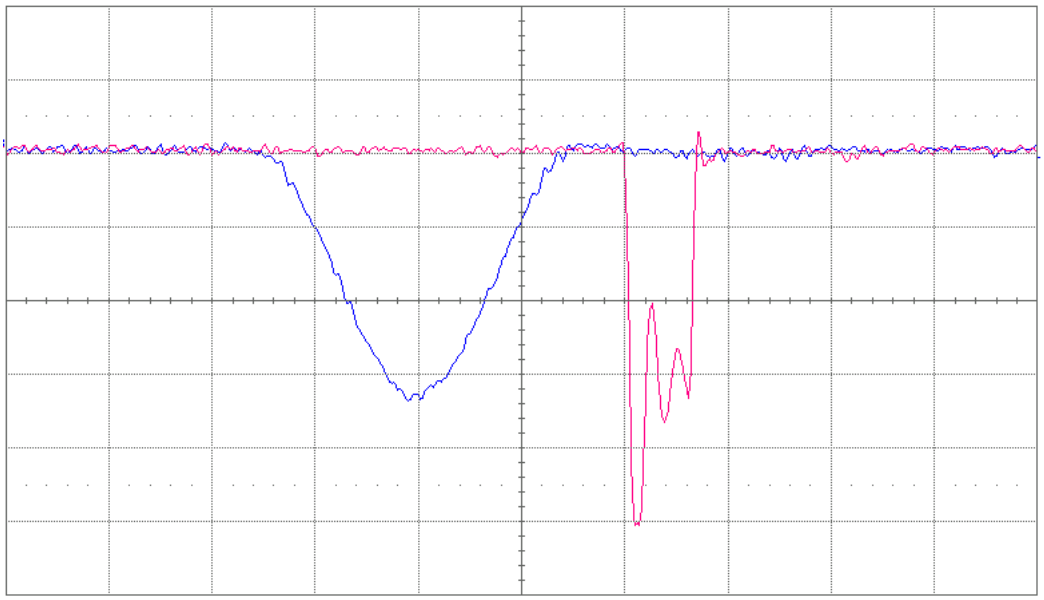

Figure 5.3: The fall time of a pulse signal (blue) generated from the function generator was 5ns. After the signal was sent into the pulse shaper, the fall time of the output signal (red) was decreased to 400ps. The pulse width also decreased from 8ns to 4ns. The timebase for this diagram is 5ns per division.

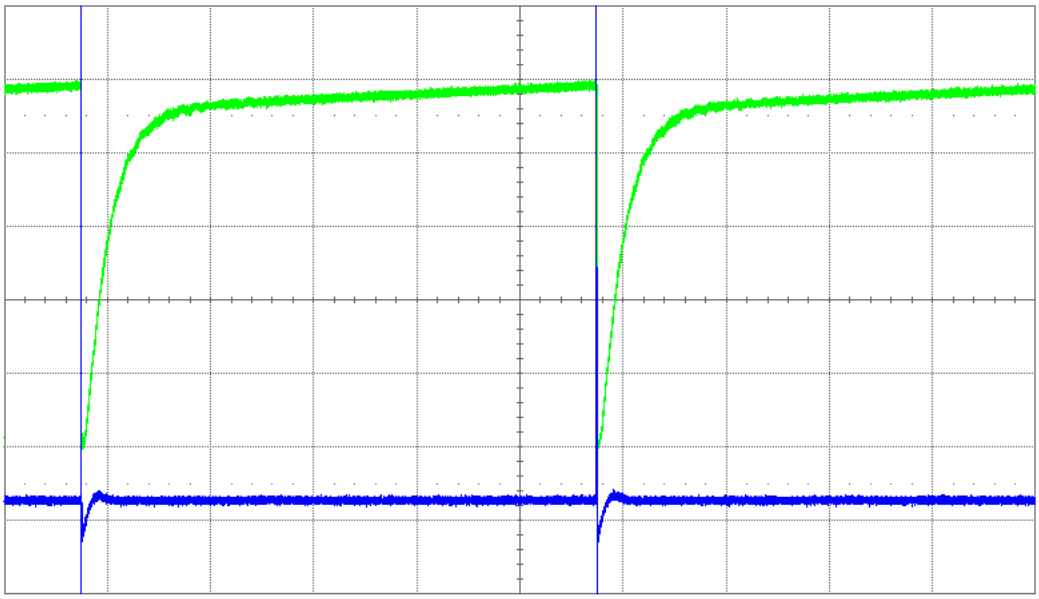

Figure 5.4: Voltage across the crystal when discharged by pulses (blue) sent into the gate of the MOSFET. The voltage (green) discharging process took (1.6±0.2)ns while the charging took 1.5μs. The timebase for this diagram is 2μs per division.

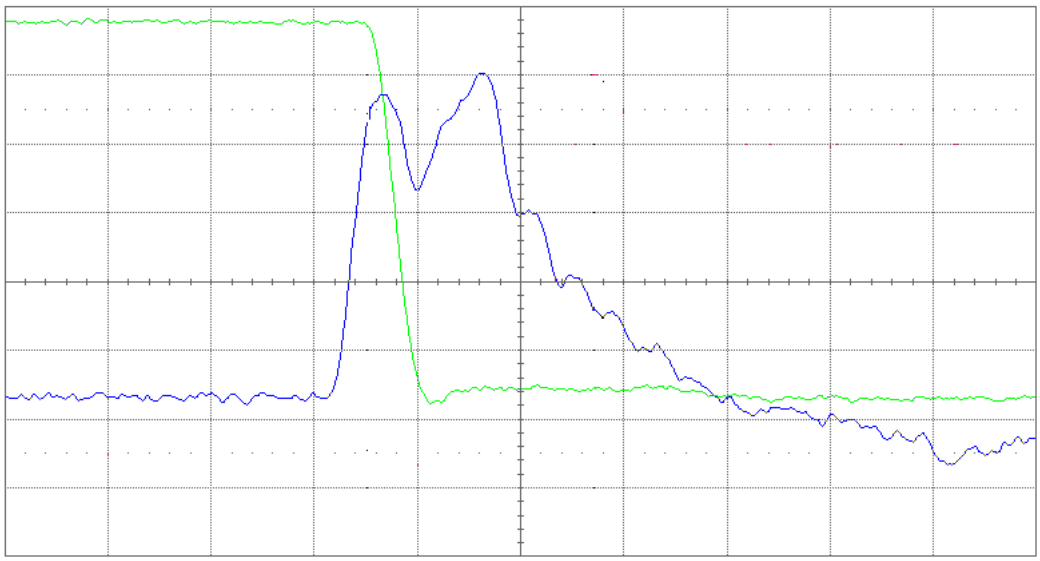

Figure 5.5: Similar in Fig(5.4), but the timebase for this diagram is 5ns per division.

constant high voltage (at least larger than half wave voltage), V is applied to the crystal to charge up the crystal. No current flows from drain to source unless the gate is brought positive with respect to the source. Once the gate is brought to positive (this is done by sending a pulse voltage into the gate), all the drain current flows to the source and the crystal starts to discharge. The model BSS 131 MOSFET was chosen because it can handle a drain source voltage up to 240V and is supposed to have a short switching time.

However, the gate voltage requires a higher voltage than the maximum voltage that could generated from the function generator. The pulses needs to be amplified by a RF amplifier (Mini-Circuits ZHL-1-2W). The RF amplifier has a gain of 33dB or the output voltage is 44.7 times higher the input voltage. The maximum gate voltage allowed is 14V and the threshold voltage is 0.8V to 2V depending on the room temperature. By increasing the gate voltage, the fall time (time where the voltage across the crystal falls from 90% of V to 10% of V) decreases until it reaches (1.6±0.2)ns. When the gate voltage increases above 10V, the discharging time does not show any further decreases. This fast switching circuit reaches the limit of the performance of the MOSFET.

The charging time depends on the capacitance. A large resistance increases the crystal charging time whereas a low resistance contributes certain oscillations before the crystal is charged up to a constant voltage. The potentiometer or variable resistor was adjusted to lower down the time constant and no oscillations were observed. The appropriate resistance was found to be 20kΩ, with a voltage rise time of approximately 1.3μs, see Fig(5.4). The capacitance of the circuit was found to be approximately 65pF. The capacitance of the crystal is given by , $C = \epsilon_0 \epsilon_r \frac{A}{d}$, where $\epsilon_0 = 8.854 \times 10^{-12} \mathrm{C}^2/\mathrm{Nm}^2$ is the permittivity of free space and $\epsilon_r = 29.5$ is the dielectric constant of Lithium Niobate. With the area, $A = 2\mathrm{cm} \times 1\mathrm{cm}$ and thickness, $d = 1\mathrm{mm}$, this gives the capacitance of the crystal, $C = 5\mathrm{pF}$. Hence, the

major contribution of the capacitance would come from the circuit structure itself.

Chapter 6

Measurement Results

The measurement of the half wave voltage was carried out by sending a low frequency saw-tooth voltage to the Lithium Niobate crystal. The half wave voltage was determined by measuring the voltage difference across the crystal where the Mach Zehnder interference undergoes from constructive to destructive or vice versa. Then, the response characterization of the optical switch (laser light shutter) will be discussed. The response was mainly limited by the capacitance and the electronics components in the circuit.

6.1 Half Wave Voltage Measurement

The measurement of half wave voltage was carried out by sending linearly polarized light at 0 degree, 45 degrees and 90 degrees into the interferometer including the polarization independent shifter to verify the consistency of the half wave voltages. In the experiment, the laser sources are 633nm Helium Neon gas laser and 690nm laser diode. As shown in Fig(6.1), the intensity out from the interferometer was measured by a photodetector connected to the digital oscilloscope. The phase modulation was carried out by applying a 50Hz saw-tooth

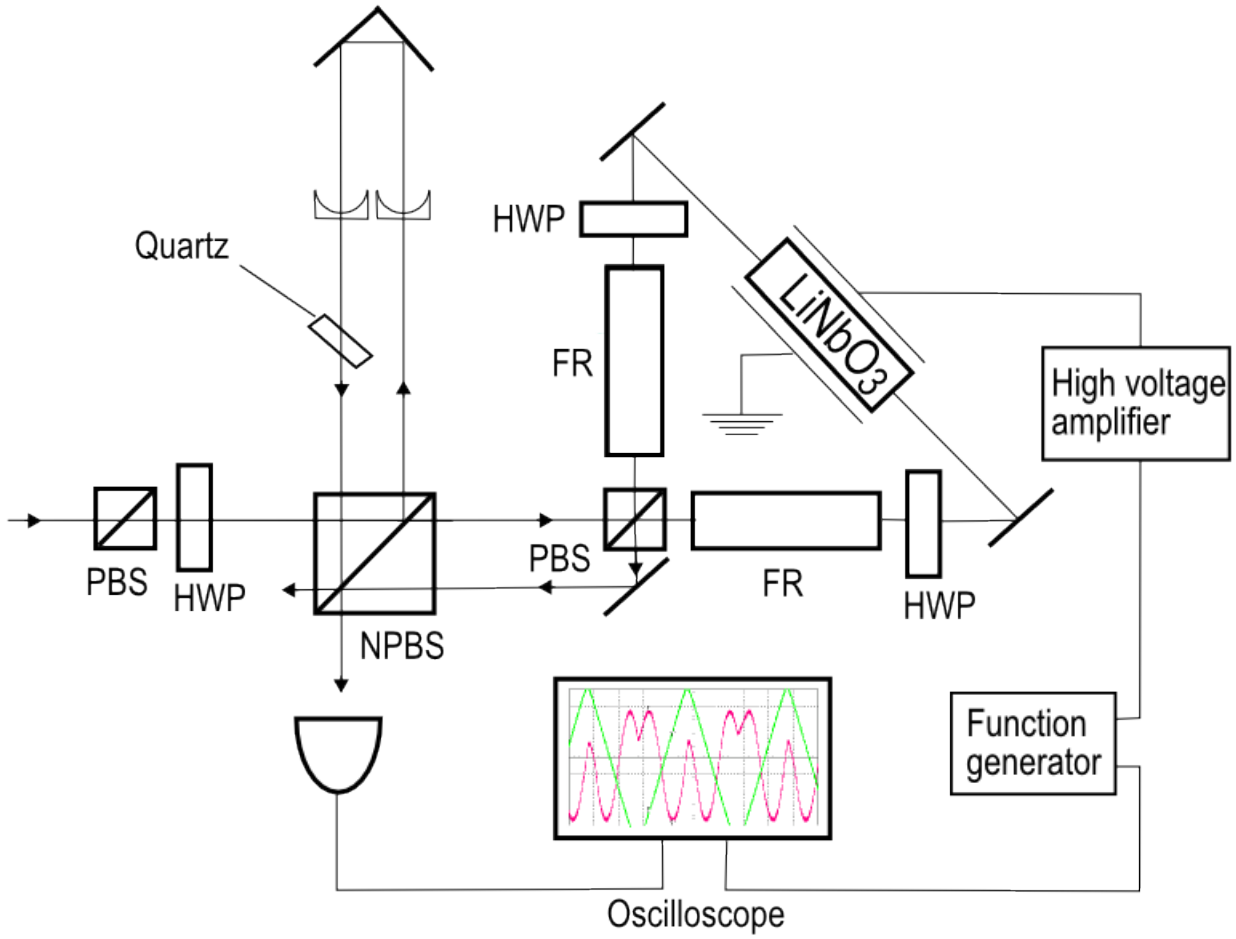

Figure 6.1: Schematic diagram for the measurement of the half wave voltage. The half wave voltage was accurately measured by probing the voltage across the crystal directly with the oscilloscope.

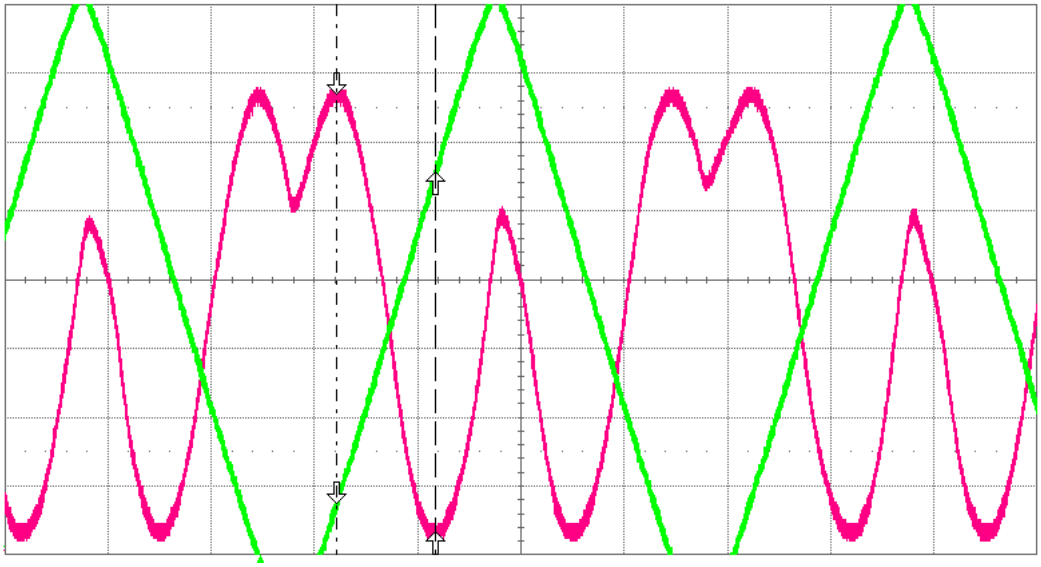

Figure 6.2: Constructive to destructive interference or vice versa under the phase modulation. The applied voltage is a 50Hz saw tooth voltage (green). The half wave voltage is the voltage difference between the minimum intensity and the maximum intensity (red). The scale for this saw tooth voltage is 20V per division.

voltage to the electrodes of the crystal. The applied voltage provided by a function generator was amplified and applied to the electrodes of the crystal. The voltage across the crystal was measured by a probe connected to the oscilloscope. The traces displayed on the oscilloscope are shown in Fig(6.2). The tables below show the results of the measurement of the half wave voltages and the visibility of the interference pattern. The visibility for the 690nm laser diode was lower compared to the one obtained with the 633nm gas laser. The reason is that the laser diode has a relatively short coherence length compared to gas laser. The stability of the current and temperature were not critical for the gas laser as well.

In this experiment, the main factor that determines the visibility would be the confocal setup. The confocal setup is the correction of the geometrical wavefront of the beam. The focus and the size of the beam were hard to optimize due to the insensitivity of the interfer-

ometer to the wavefront correction.

Have wave voltage of 633nm gas laser		
Polarization	$(V_\pi \pm 2)$V	Visibility
0^o	97V	96%
45^o	96V	95%
90^o	96V	96%

Have wave voltage of 690nm laser diode		
Polarization	$(V_\pi \pm 2)$V	Visibility
0^o	108V	91%
45^o	105V	92%
90^o	109V	93%

The polarization independent phase shifter works according to the plan. After verifying that the half wave voltage is consistent with the theorectical calculation, the next step is to proceed to the fast switch characterization.

6.2 Characterization of the Optical Switch

6.2.1 Fast Switching Time

In chapter 5, the response of the voltage charging and discharging process has been characterized. These processes are directly related to the intensity modulation due to the phase shift modulated by the voltage across the crystal. In this section, for a optical switch, the

response of the intensity modulation needs to be characterized.

A fast optical switch or laser light shutter is a device that switches the optical beam 'ON' or 'OFF'. A mechanical light shutter is unable to switch the light on to off or vice versa in a few nanoseconds. However, the crystal inside the electro optic modulator has a very fast response time, in the order of picoseconds. The combination of the interferometer and electro optic modulator would be a fast laser light shutter.

As mentioned in the previous chapter, a constant high voltage (at least half wave voltage) is continuously applied across the crystal. Pulses are sent into the gate of the MOSFET to discharge the crystal, so the light undergoes π phase shift. This gives rise to the change from constructive to destructive interference or vice versa. The characteristic time of the discharging process depends on the gate voltage which can be controlled by the pulses. Since the discharging process takes less than 2ns, the intensity modulation would be expected to lead to an optical signal with a bandwidth of 250MHz. A fast photodiode (Hamamatsu S5973 silicon PIN photodiode) with a amplifier were built to measure the fast changing intensity. The bandwidth of the photodiode is 1GHz with the reverse bias voltage at least 3.3V (according to the data sheet provided by the manufacturer).

Fig(6.3) shows that the fall time for the discharging process and the intensity rise time measured at the photodiode were consistent, the time measured was (1.6±0.2)ns. The rise time of the intensity could be accurately measured by using the piezo screw to move the mirror until the the two beams were destructively interfered before the discharging process. When the crystal started to discharge, the intensity detected would increase from minimum to maximum. The stability of the interferometer would be the main factor affects the intensity rise time.

However, the time when the intensity rises is not consistent with the time when the

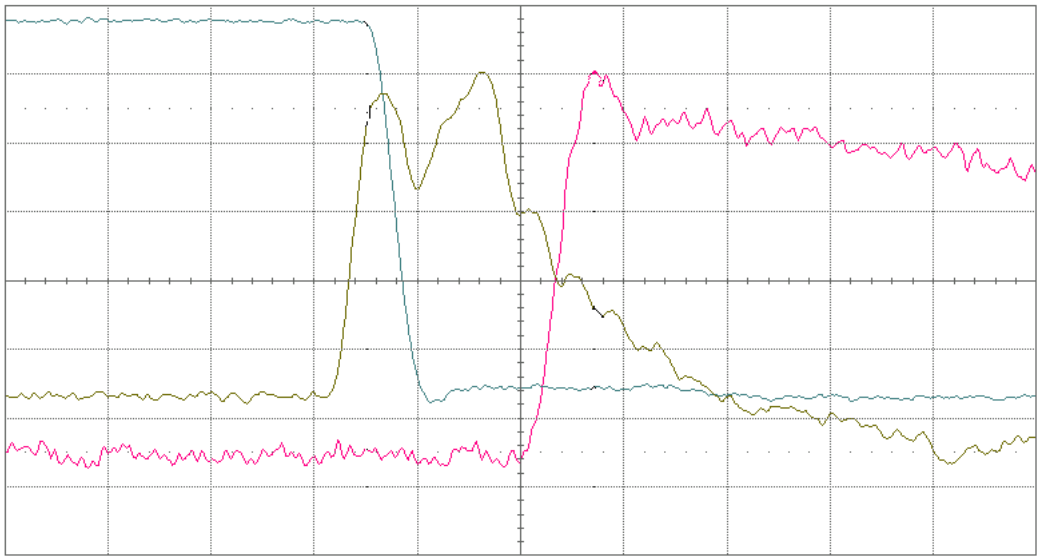

Figure 6.3: The pulse voltage (green) was increased to drive the discharging process. At this moment, the voltage (blue) across the crystal dropped changing the phase difference between the laser beam in the interferometer. Hence, the intensity (red) was increased from minimum to maximum due to the interference effect.

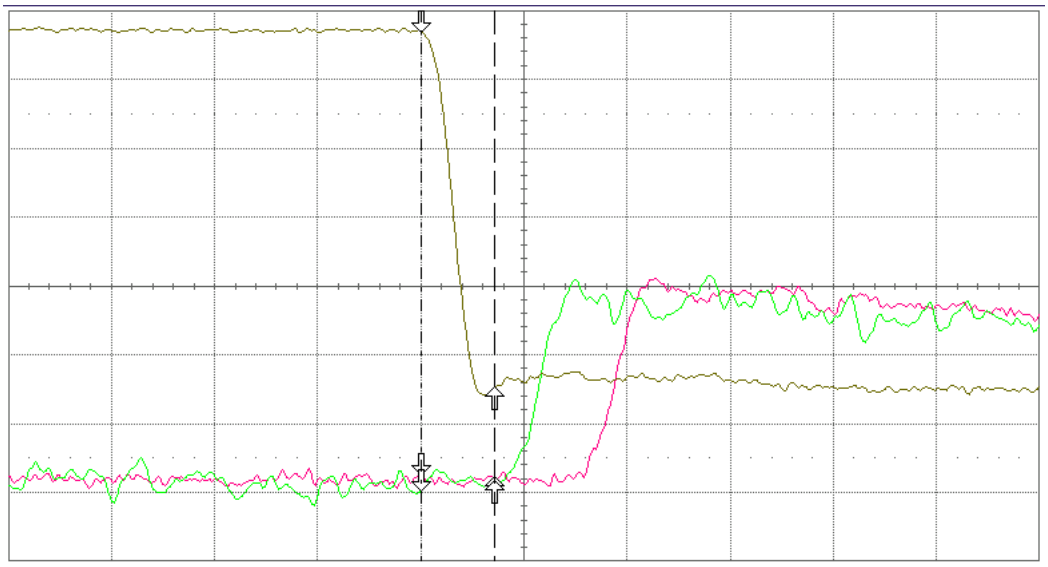

Figure 6.4: The delay was decreased from 8ns to 4ns after using a shorter cable.

voltage across the crystal starts to discharge. The rise of the intensity was delayed about 8ns with respect to the discharging process. This was due to the length of the interferometer and the length of the cable connected between the photodetector and the oscilloscope. The laser beam that is modulated inside the crystal travels a distance of approximately 40cm before it reaches the photodetector. This travelling distance gives the delay of at least 1ns. This could be proved by probing the intensity signal using a shorter cable. Fig(6.4) shows the delay time was decreased after using a shorter probe.

6.2.2 Repetition Rate

The time constant, $\tau = RC$ for recharging the crystal is largely determined by the capacitance of the circuit. At very low repetition frequencies, $f << (RC)^{-1}$, the voltage drop across the capacitor is very nearly equal to the applied voltage and there is a very small drop in voltage across the resistor. However, if $f > (RC)^{-1}$, only a fraction of the voltage is applied to the crystal. Therefore, the limitation can be significantly reduced by decreasing the capacitance of the device, or choosing a lower value for the resistor. This is the reason why an integrated optics modulator is able to achieve superior performance. In general, when $f_0 = (CR)^{-1}$, the voltage across the modulating crystal is only $\frac{V}{\sqrt{2}}$. By definition, f_0 is defined as cutoff frequency of the modulator.

A high voltage 100V was constantly applied across the crystal. The voltage across the crystal was probed with respect to the frequency of the pulses. The result in Fig(6.5) shows that the actual voltage across the crystal decreased to almost zero when the frequency of the pulses reached more than 5MHz. The largest pulse frequency or repetition rate was found to be 100kHz. Fig(6.6) shows the optical switch was operated with a repetition rate of 100kHz.

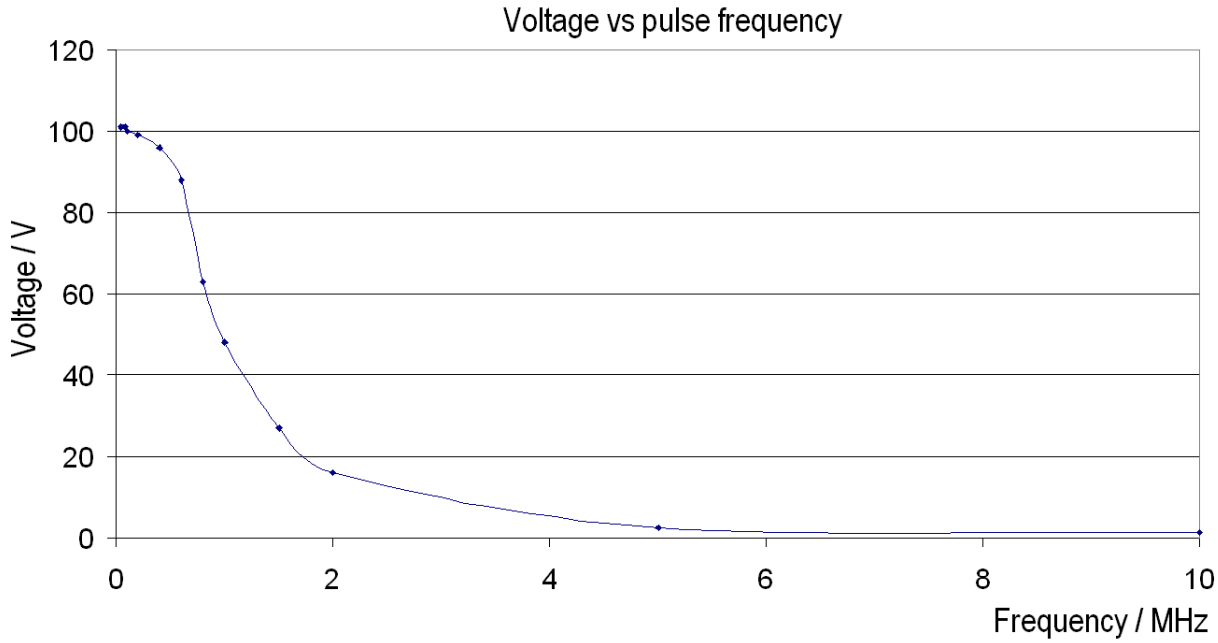

Figure 6.5: The actual voltage across the crystal decreased as the pulse repetition rate was increased.

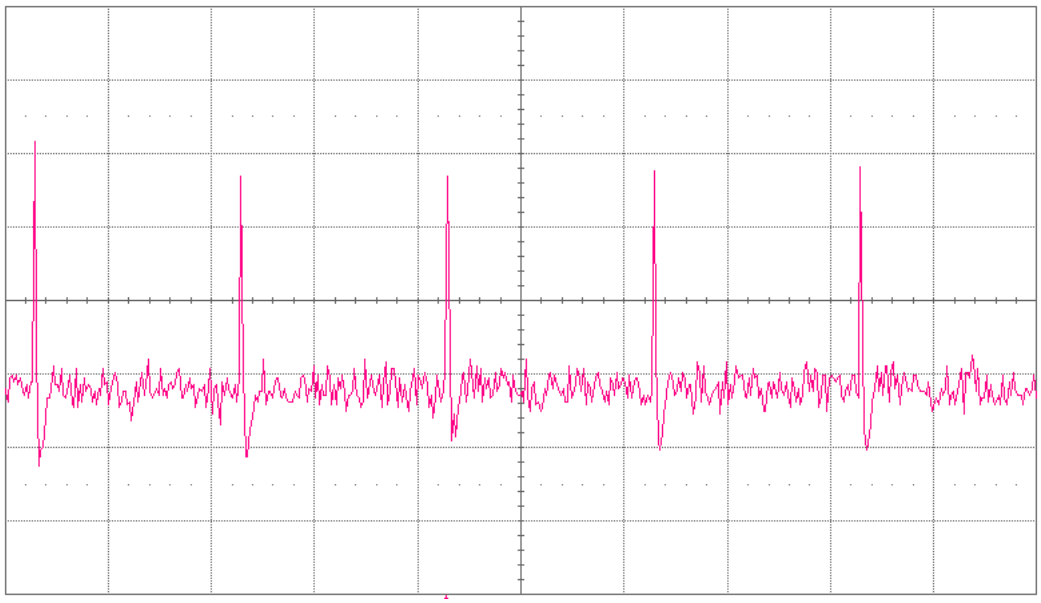

Figure 6.6: The optical switch was operated with a repetition rate of 100kHz. The sharp peaks correspond to the ON state of a laser light shutter. The timebase for this diagram is 5μs per division.

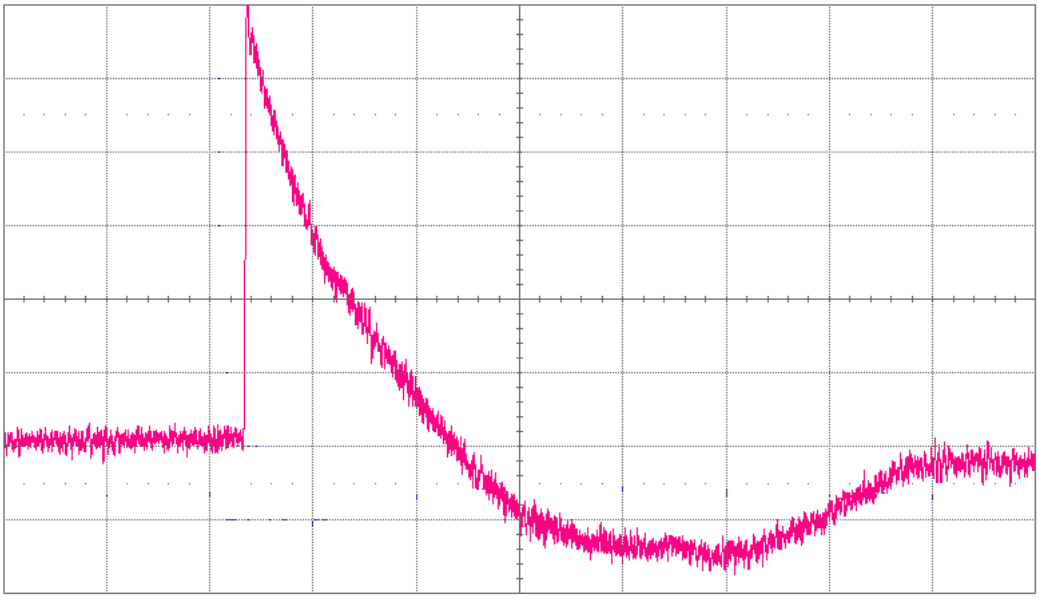

Figure 6.7: The characteristic time for the shutter switches the light on to off is limited by the recharging time constant. The timebase for this diagram is 100ns per division.

Main parameters of the fast light shutter	
Rise time (10%-90%)	less than 2ns (typical is 1.6ns)
Fall time (10%-90%)	less than 2μs
Visibility	96% (HeNe laser)
Repetition rate	100kHz

The rise time is limited by the performance of the MOSFET, while the fall time is limited by the high voltage amplifier. The experiment is still in the stage of improving the shutter speed performance. The electronic circuit structure can be improved by using a better MOSFET or reducing the total capacitance. From Fig(6.7), the maximal repetition rate depends on the charging time constant of the capacitance. A lower recharging resistance decreases the charging time constant, but it gives a large current. The current is limited by the capability of the MOSFET.

The broadband modulator that built in this project can be further improved by designing a resonant circuit. In resonant phase modulator, the crystal is combined with an inductor to form a resonant tank circuit. On resonance, the circuit looks like a resistor whose value depends on the loss of the inductor. A transformer is used to match this resistance to the 50ohm driving impedance. This results in the voltage across the crystal can be more than few times larger than the input drive voltage. This leads to reduced input drive voltage and larger modulation depths compared to the broadband modulators.

Chapter 7

Conclusions & Future Work

The fast polarization independent phase shifter with a laser light shutter can be operated in less than 2ns. The light shutter presented in this work is able to achieve its performance even with a laser source with a short coherence length. A long coherence length using the Helium Neon gas laser gives a superior performance, the visibility of the interferometer would be 96% as reported. Ultimately, the fast switching time depends on the electronic circuit, the capacitance of the crystal and the stability of the interferometer. The shutter performance depends on the wavelength of the laser sources since a longer wavelength requires a larger half wave voltage. This decreases the shutter speed and the repetition rate.

The down converted light generated from the spontaneous parametric down conversion (SPDC) process will be the next light source to test the performance of the device built in this experiment. This process generates one pair or two down converted photons in the entangled state. For the application, one would like to direct one of the members of the pair between several alternative measurements without affecting its polarization state. The conditional measurement would increase the efficiency of the quantum computing in the future.

Chapter 8

Appendix

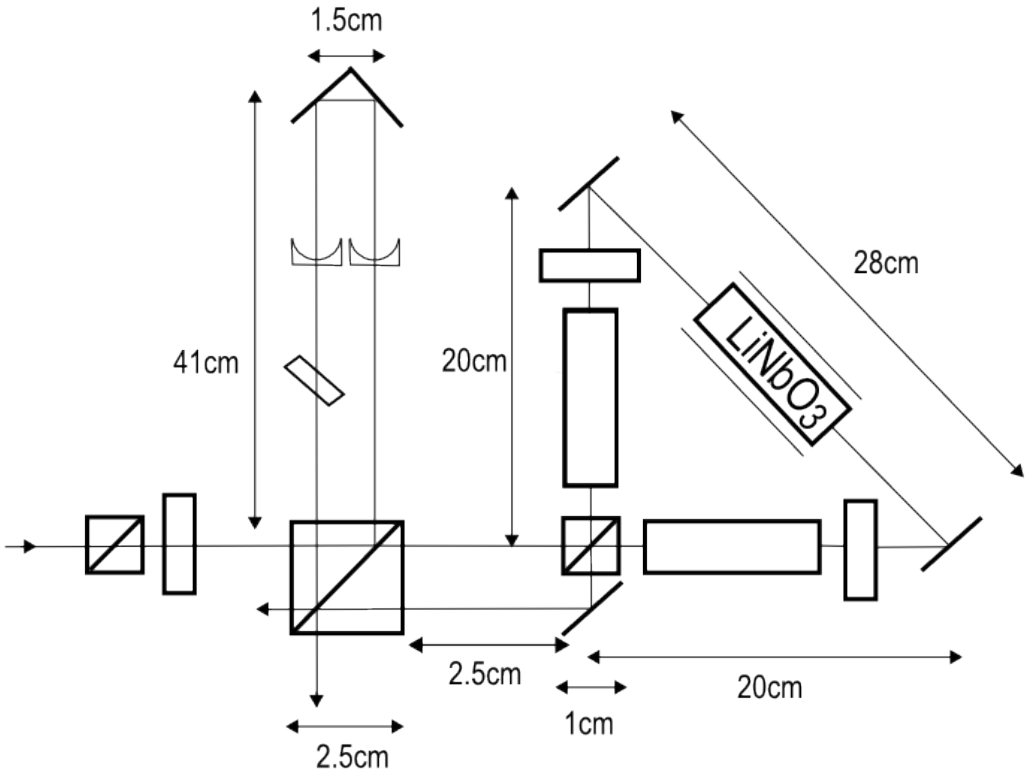

Figure 8.1: The diagrams shows the geometrical setup of the interferometer in this experiment (not to scale).

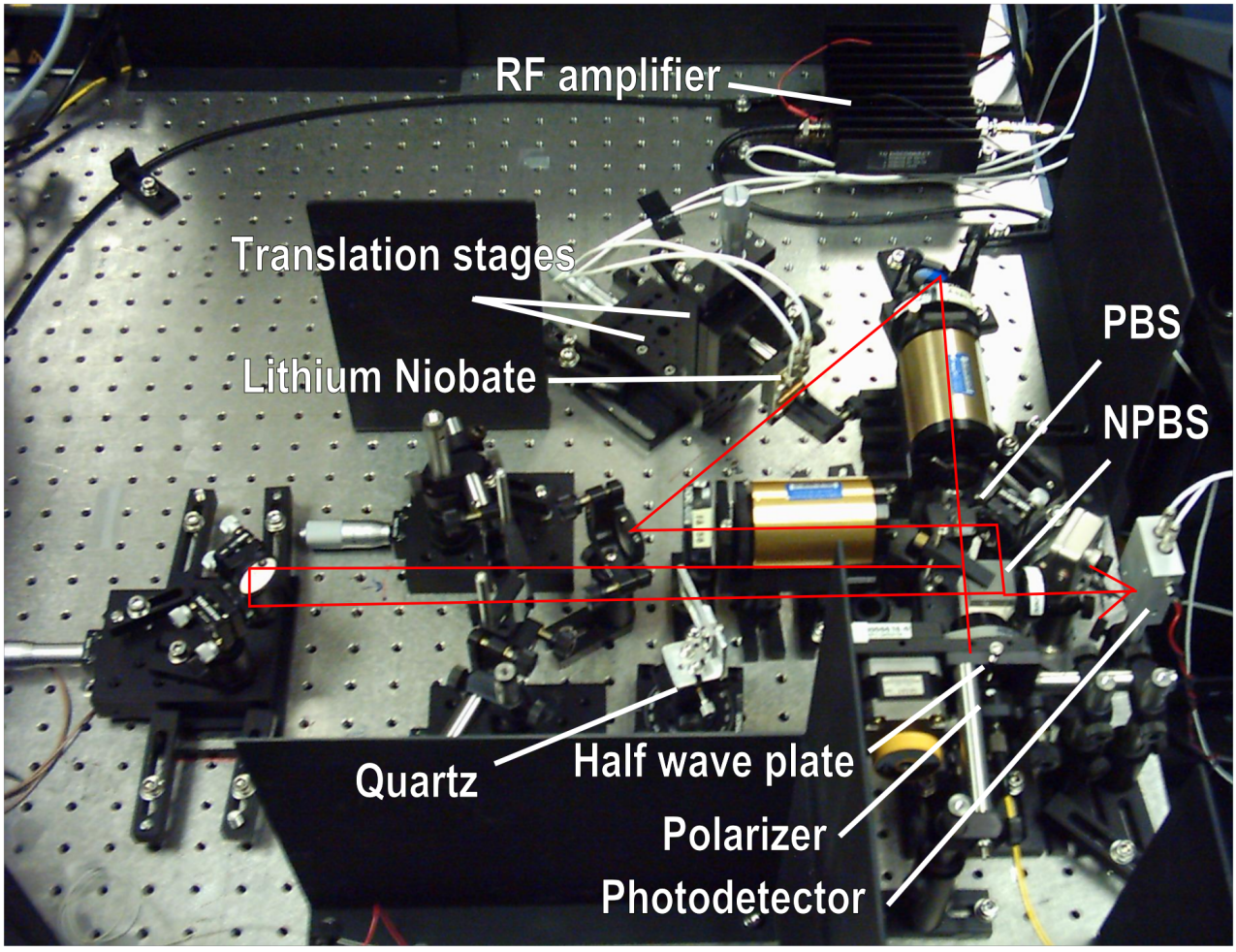

Figure 8.2: Complete experimental setup.

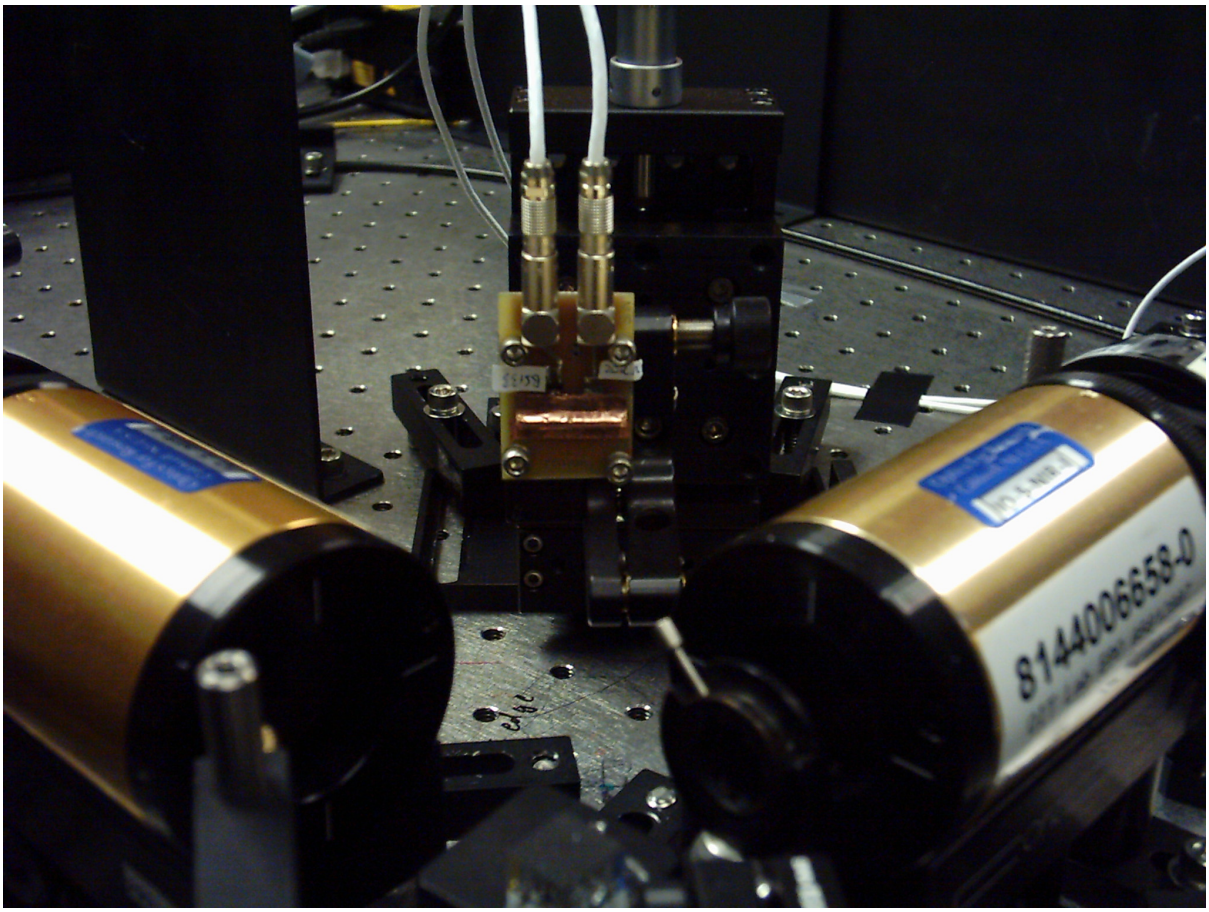

Figure 8.3: The Lithium Niobate crystal together with the circuit board was mounted on a beam splitter mount.

Bibliography

[1] Ivan P. Kaminow, *An Introduction To Electrooptic Devices*, Academic Press, (1974)

[2] C. S. Adams, *Rev. Sci. Instrum.* **71**, 59 (2000)

[3] J F McCann, J Pezy, P Wilsen, *J. Phys. E: Sci. Instrum.* **15**, 322 (1982)

[4] A. Yariv, *Quantum Electronics*, John Wiley & Sons, 3rd ed. 1989, pp.87

[5] R. V. Schmidt, I. Kaminow, *Appl. Phys. Lett.* **25**, 458 (1974)

[6] Fernando Agullo-Lopez, Jose Manuel Cabrera, Fernando Agullo-Rueda, *Electrooptics : Phenomena, Materials And Applications*, Academic Press, 1994, pp.138

[7] L. Thylen, *J. Lightwave Technol.*, LT-6:847 (1988)

[8] A. Yariv, P. Yeh, *Optical Waves in Crystals : Propagation and Control of Laser Radiation*, John Wiley & Sons, 2003, pp.237

[9] Christopher C. Davis, *Laser and Electro-Optics : Fundamentals and Engineering*, Cambridge University Press, 1996, pp.483

[10] Bahaa E. A. Saleh, Malvin Carl Teich, *Fundamentals of Photonics*, John Wiley & Sons, 1991, pp.715

[11] I. P. Kaminow, E. H. Turner, *Appl. Opt.* **5**, 1612 (1966)

[12] Ajoy Ghatak, K. Thyagarajan, *Optical Electronics*, Cambridge University Press, 1989, pp.477

[13] F. T. S. Yu, Xiangyang Yang, *Introduction To Optical Engineering*, Cambridge University Press, 1997, pp.159

[14] W. H. Steel, *Interferometry*, Cambridge University Press, 1983, pp.236

[15] Clifford R. Pollock, *Fundamentals Of Optoelectronics*, Prentice Hall, 1995, pp.243

[16] S. Desmond Smith, *Optoelectronic Devices*, Irwin, 1995, pp.509

[17] A. Ashkin, G. D. Boyd, J. M. Dziedzik, R. G. Smith, A. A. Ballman and K. Nassau, *Appl. Phys. Lett.*, **9**, 72 (1966)

[18] T. J. Hall, R. Jaura, L. M. Connors, P. D. Foote, *The Photorefractive Effect - A Review*, Prog. Quantum Elect. 10, pp.77

[19] Paul Horowitz, Winfield Hill, *The Art of Electronics*, Cambridge University Press, 2nd ed. 1997, pp.114